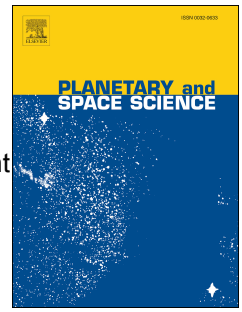

The HABIT (HabitAbility: Brine Irradiation and Temperature) environmental instrument for the ExoMars 2022 Surface Platform

Javier Martin-Torres, Maria-Paz Zorzano, Alvaro Soria-Salinas, Miracle Israel Nazarious, Samuel Konatham, Thasshwin Mathanlal, Abhilash Vakkada Ramachandran, Juan-Antonio Ramirez-Luque, Roberto Mantas-Nakhai

PII: S0032-0633(20)30061-1

DOI: https://doi.org/10.1016/j.pss.2020.104968

Reference: PSS 104968

To appear in: *Planetary and Space Science*

Received Date: 12 February 2020

Revised Date: 1 May 2020

Accepted Date: 5 May 2020

Please cite this article as: Martin-Torres, J., Zorzano, M.-P., Soria-Salinas, A., Nazarious, M.I., Konatham, S., Mathanlal, T., Ramachandran, A.V., Ramirez-Luque, J.-A., Mantas-Nakhai, R., The HABIT (HabitAbility: Brine Irradiation and Temperature) environmental instrument for the ExoMars 2022 Surface Platform, *Planetary and Space Science* (2020), doi: https://doi.org/10.1016/j.pss.2020.104968.

CRediT author statement

Javier Martín-Torres: Conceptualization, Methodology, Supervision, Investigation, Writing- Original draft preparation**,** Funding acquisition, Resources, Project Administratio; **María-Paz Zorzano:** Conceptualization, Methodology, Supervision, Investigation, Writing- Original draft preparation**,** Funding acquisition, Resources, Project Administration; **Alvaro Soria-Salinas:** Formal Analysis, Investigation, Visualization, Writing - Review & Editing,; **Miracle Israel Nazarious:** Formal Analysis, Investigation, Visualization, Writing - Review & Editing; **Samuel Konatham:** Formal Analysis, Investigation, Visualization, Writing - Review & Editing; **Thasshwin Mathanlal:** Formal Analysis, Investigation, Visualization, Writing - Review & Editing; **Abhilash Vakkada Ramachandran:** Formal Analysis, Investigation, Visualization, Writing - Review & Editing; **Juan-Antonio Ramirez-Luque:** Software, Writing- Reviewing and Editing; **Roberto Mantas-Nakhai:** Software, Writing- Reviewing and Editing

Draft for Planetary and Space Science

The HABIT (HabitAbility: Brine Irradiation and Temperature) environmental instrument for the ExoMars 2022 Surface Platform

Authors

Javier Martin-Torres* (1,2), Maria-Paz Zorzano* (3,1), Alvaro Soria-Salinas (1), Miracle Israel Nazarious (1), Samuel Konatham (1), Thasshwin Mathanlal (1), Abhilash Vakkada Ramachandran (1), Juan-Antonio Ramirez-Luque (1) and Roberto Mantas-Nakhai (1).

1. Atmospheric Science, Department of Computer Science, Electrical and Space Engineering, Luleå University of Technology, Luleå, 97 187 Sweden
2. Instituto Andaluz de Ciencias de la Tierra (CSIC-UGR), 18100 Granada, Spain
3. Centro de Astrobiología (CSIC-INTA), Torrejón de Ardoz, 28850 Madrid, Spain

*: JMT and MPZ led this work

Abstract

The HABIT (HabitAbility: Brine Irradiation and Temperature) instrument is a European payload of the ExoMars 2022 Surface Platform Kazachok that will characterise the present-day habitability at its landing place in Oxia Planum, Mars. HABIT consists of two modules: (i) EnvPack (Environmental Package) that monitors the thermal environment (air and ground), the incident ultraviolet radiation, the near surface winds and the atmospheric dust cycle; and (ii) BOTTLE (Brine Observation Transition To Liquid Experiment), an In-situ Resource Utilization instrument to produce liquid water for future Mars exploration. BOTTLE will be used also to investigate the electrical conductivity properties of the martian atmosphere, the present-day atmospheric-ground water cycle and to evaluate if liquid water can exist on Mars in

the form of brines, and for how long. These variables measured by HABIT are critical to determine the present and future habitability of the martian surface. In this paper, we describe in detail the HABIT instrument and sensors, together with the calibration of its Flight Model (FM) and the Engineering Qualification Model (EQM) versions. The EnvPack module has heritage from previous missions operating on the surface of Mars, and the environmental observations of its sensors will be directly comparable to those delivered by those missions. HABIT can provide information of the local temperature with ±0.2°C accuracy, local winds with ± 0.3 m/s, surface brightness temperature with ±0.8°C, incident UV irradiance with 10% error of its absolute value in the UV-A, UV-B, UV-C ranges, as well as in the total UV-ABC range, and two additional wavebands, dedicated to ozone absorption. The UV observations can be used to derive the total opacity column and thus monitor the dust and ozone cycles. BOTTLE can demonstrate the hydration state of a set of four deliquescent salts, which have been found on Mars (calcium chloride, ferric sulphate, magnesium perchlorate and sodium perchlorate) by monitoring their electric conductivity (EC). The EC of the air and the dry salts under Earth ambient, clean room conditions is of the order of 0.1 μScm^{-1}. We have simulated HABIT operations, within an environmental chamber, under martian conditions similar to those expected at Oxia Planum. For dry, CO_2 atmospheric conditions at martian pressures, the air EC can be as low as 10^{-8} μScm^{-1}, however it increases with the relative humidity (RH) percentage. The laboratory experiments show that after an increase from 0 to 60% RH within a few hours, the EC of the air increased up to 10^{-1} μScm^{-1}, magnesium perchlorate hydrated and reached values of 10 μScm-1, whereas calcium chloride deliquesced forming a liquid state with EC of 10^{2} μScm^{-1}. HABIT will operate with a regular cadence, through day and night. The Electronic Unit (EU) is protected with a heater that is activated when its temperature is below -33℃ and disabled if the temperature of the surface platform rises above -30℃. Additionally, the heaters of the BOTTLE unit can be activated to dehydrate the salts and reset the

experiment. HABIT weighs only 918 g. Its power consumption depends on the operation mode and internal temperature, and it varies between 0.7 W, for nominal operation, and 13.1 W (when heaters are turned on at full intensity). HABIT has a baseline data rate of 1.5 MB/sol. In addition to providing critical environmental observations, this light and robust instrument, will be the first demonstrator of a water capturing system on the surface of Mars, and the first European In-Situ Resource Utilization in the surface of another planet.

Keywords: Mars, ExoMars, Surface Platform, instrumentation, habitability, water, ISRU, Atmosphere, regolith, brines, astrobiology

1 Introduction

The search for present life and habitability on Mars is conditioned by the availability of liquid water. Also, the future potential exploration of Mars by humans is conditioned by the availability to produce in-situ critical products such as water, oxygen or propellant. Recently it has been shown that liquid water can be stable on Mars in the form of brines (Martín-Torres et al., 2015). Two other environmental conditions constrain the habitability of the near surface of Mars: the thermal range and the ultraviolet radiation dose (Rummel et al., 2014). The quest about the habitability of present-day Mars is still open and a crucial aspect for the future human space exploration. The HabitAbility: Brines, Irradiance and Temperature (HABIT) instrument, will focus on this subject. HABIT is one of the two European payloads of the Surface Platform *Kazachok* that is part of the Exomars 2022 mission to Mars. ExoMars is a joint program by the European Space Agency (ESA) and the Russian Space Agency (Roscomos) which comprises two missions, in 2016 and 2022. The 2016 mission is called Trace Gas Or-

biter (TGO), which is now in operation on Mars monitoring traces gases, such as methane and water in the atmosphere (Vandaele et al., 2019; Korablev et al. 2019). In addition to its own scientific goals, TGO will serve as relay for the ExoMars 2022 surface mission. This mission, to be launched in 2022 (final windows date to be decided), shall land at Oxia Planum (18.20°N, 335.45°E) on Mars, a plain with an elevation more than 3,000 metres below the martian mean. It will search for signs of present or past life on Mars with its rover and surface platform and will bring the first European/Russian rover and Surface Platform (SP) to the surface of Mars.

HABIT will characterize the habitability at the landing site of the mission, Oxia Planum (Bhardwaj et al., 2019; Fonseca et al., 2019), in terms of Ultra-Violet (UV) radiation, air and ground temperature (T), as well as liquid water availability and in-situ atmospheric water extraction usage. It will also monitor the near surface winds, and the atmospheric dust cycle. Additionally, it will provide measurements of the air electric conductivity (which changes with the relative humidity of the air) and over time, when dust is accumulated in one of the open cells of HABIT, it will provide an estimate of the electric conductivity of the dust. Having in-situ information about these processes is also key for the design of future missions to Mars.

The ExoMars mission will pursue one of the outstanding questions of our time by attempting to establish whether life ever existed or is still active on Mars today (Vago et al., 2017). This is specifically the goal of the payloads of the rover (http://exploration.esa.int/mars/45103-rover-instruments/) and HABIT, mounted on the Surface Platform, will contribute to this later goal, namely it will assess the present-day habitability of Oxia Planum, in terms of key environmental variables. The thermal ranges, water avail-

ability and UV radiation doses are critical environmental parameters that condition the habitability of Mars. The correct characterization of the wind and heat fluxes on Mars are also important for the operational performance of spacecraft platforms and for our understanding of the boundary layer dynamics. The dust cycle and the electric conductivity may also be potential hazards to the future exploration of Mars.

Finding unequivocal proofs of liquid water on present day Mars is a prominent domain of Mars research with implications for the conditions promoting habitability and the future of Mars exploration as well as for the definition of planetary protection protocols (Bhardwaj et al., 2019; Rummel et al., 2014). HABIT includes the BOTTLE (Brine Observation Transition To Liquid Experiment) module to capture at night-time atmospheric water by hydration and deliquescence of salts, and three environmental sensors – Ground Temperature Sensor (GTS), Air Temperature Sensor (ATS), and UltraViolet Sensor(UVS) – devoted to monitoring the full diurnal and seasonal variations of the ground and air temperature, the near surface winds and the UV irradiance. BOTTLE also includes two open containers to study the electrical conductivity properties of the martian atmosphere. The information provided by the three environmental sensors of HABIT will allow to constrain the habitability at the landing site in terms of metabolic and reproduction temperature, calculating the heat-flux and the UV biological dose, study the atmosphere/surface water interchange, providing information about winds (which shall be useful also for the rover drilling and sampling operations and for validation of global and meso-scalar circulation models), about thermal inertia and subsurface thermal profile and hydration level complementing the studies of the other platform and rover instruments. The analysis of the measured UV irradiance may also be used to provide the concentration of the atmospheric trace gas ozone (complementing orbiter observations from NOMAD-TGO) and the total column of dust or opacity (providing continuous monitoring of

the dust cycle). Additionally, the environmental observations of HABIT will be compared with those of REMS on board the Curiosity rover of the Mars Science Laboratory mission (Gómez-Elvira et al., 2012; Gómez-Elvira et al., 2014) and of other environmental sensors which are designed with heritage of REMS, such as Twins on InSight and MEDA on the Mars 2020 NASA Perseverance rover. The BOTTLE module is furthermore designed as an ISRU (In-situ Resource Utilization) demonstrator that shall quantify the amount of water (and derived products such as H_2 and O_2) available for future landed missions on Mars. Thus, HABIT will allow for extra long-term climate and atmospheric monitoring and will provide an unequivocal proof, for the first-time, of the existence of liquid water on Mars, while demonstrating the ISRU capabilities of salts.

The scientific objectives of the ExoMars program are defined as follows (Vago et al., 2017): 1) To search for signs of past and present life on Mars; 2) To investigate the water/geochemical environment as a function of depth in the shallow subsurface; 3) To study martian atmospheric trace gases and their sources; and 4) To characterize the surface environment.

The scientific objectives of HABIT are:

1. Investigate the habitability of the landing site in terms of the three most critical environmental parameters for life as we know it: availability of liquid water, UV biological dose and thermal ranges (on Earth, microbial metabolism has only been found above 240 K and reproduction above 255 K);

2. Provide environmental information (air and ground temperature, ground relative humidity (RH) and UV irradiance), to investigate the atmosphere/regolith water interchange, the subsurface hydration, as well as the ozone, water and dust atmospheric cycle and the convective activity of the boundary layer;

3. Demonstrate an In-Situ Resource Utilization technology for future Mars exploration.

4. The clear detection of a high conductivity signal within BOTTLE would reveal that the deliquescence mechanism is in effect on Mars. This would have major implications. First, it would confirm the possibility of a present-day atmosphere-regolith interaction that may lead to the formation of briny mixtures which, in the case of deep slopes may be observed from orbit through large-scale features like Recurrent Slope Lineae. This is still a controversial topic, i.e., see Bhardwaj et al. (2019) and Dundas et al. (2020). The identification of the transient liquid water and its stability time scales would open the discussion about the possibility of life in present day Mars and various other key points linked with the future human exploration. It is also expected that the demonstration of the formation of liquid brine would have implications on the definition of special regions defined for planetary protection purposes.

HABIT is designed to be a robust, small and light instrument that complies with the ExoMars science objectives and priorities:

1. Search for signs of past and present life on Mars: The clear detection of transient liquid conditions is key to assessing the possibility of present life on Mars, since water is a requirement for life as we know it. The determination of the surface and subsurface

thermal range will allow evaluating if the landing site complies with the known thermal limits of terrestrial microbial reproduction and metabolism;

2. Investigate the water/geochemical environment as a function of depth in the shallow subsurface: The investigation of the diurnal cycle of water, the formation of frost and the hydration of salts at the surface and the subsurface will allow to investigate the water environment as a function of depth in the upper meters of the regolith where the diurnal and annual thermal wave act;

3. Study martian atmospheric trace gases and their sources: Water is a trace gas on Mars and HABIT will investigate the water cycle, its sources (when released from the soil dehydration) and sinks (absorbed by the soil). O_3 is a trace gas produced by atmospheric photolysis with UV, the concentration of O_3 can be monitored with the UV sensor, its cycle anti-correlates with atmospheric water. The UV irradiance also drives the concentration of other minor gases that are produced from CO_2: CO, O_2;

4. Characterize the surface environment: HABIT will evaluate the habitability of the near surface environment, in terms of thermal range, water availability and UV dose. It will also provide critical environmental information regarding the dust cycle, and wind activity, as well as the thermal tide response, heat-fluxes and planetary circulation at the boundary layer.

This paper is aimed at describing the HABIT instrument, its operation and sensing elements and the calibration and validation of the HABIT Flight Model (FM) and HABIT Engineering Qualification Model (EQM) which have been developed by Omnisys, Sweden, and the Group

of Atmospheric Science at Luleå University of Technology (LTU), with support of the Swedish National Space Agency (SNSA). Following ESA policy, the HABIT data will be released for public use and archived at Roscosmos/IKI and mirrored at the Planetary Science Archive (PSA), and thus this document shall serve as reference for the future scientific analysis of the HABIT data. It is also the intention of this article to describe the potential and limitations of the instrument, so that the data can be interpreted correctly.

2. Instrument design

HABIT and its modules are shown in Figure 1. The dimensions of the Container Unit (CU) the Electronic Unit (EU) are 150 mm x 63 mm x 43 mm and 172 mm x 172 mm x 55 mm (L x B x H) respectively. The Electronic Unit (EU) is protected with a heater that is activated when its temperature is below -33℃ and disabled if the temperature of the Surface Platform rises above -30℃. This implies that the CU, at nighttime when the RH% peaks, will be warmer than the martian ground. The instrument weights 918 g; requires a power consumption that ranges between 0.7 and 13.0 W (when the heaters are activated) and a baseline data rate of 1.5 MB/sol. The CU, the lid and the filter holder are manufactured in aluminium, the electrodes are made of gold, to prevent corrosion, and the magnetic rings around the UV photodiodes are made of samarium cobalt. The instrument measures at 1 Hz, on its nominal operation mode, during five minutes at the beginning of each hour. It can also operate in extended mode, within programmable continuous periods of time.

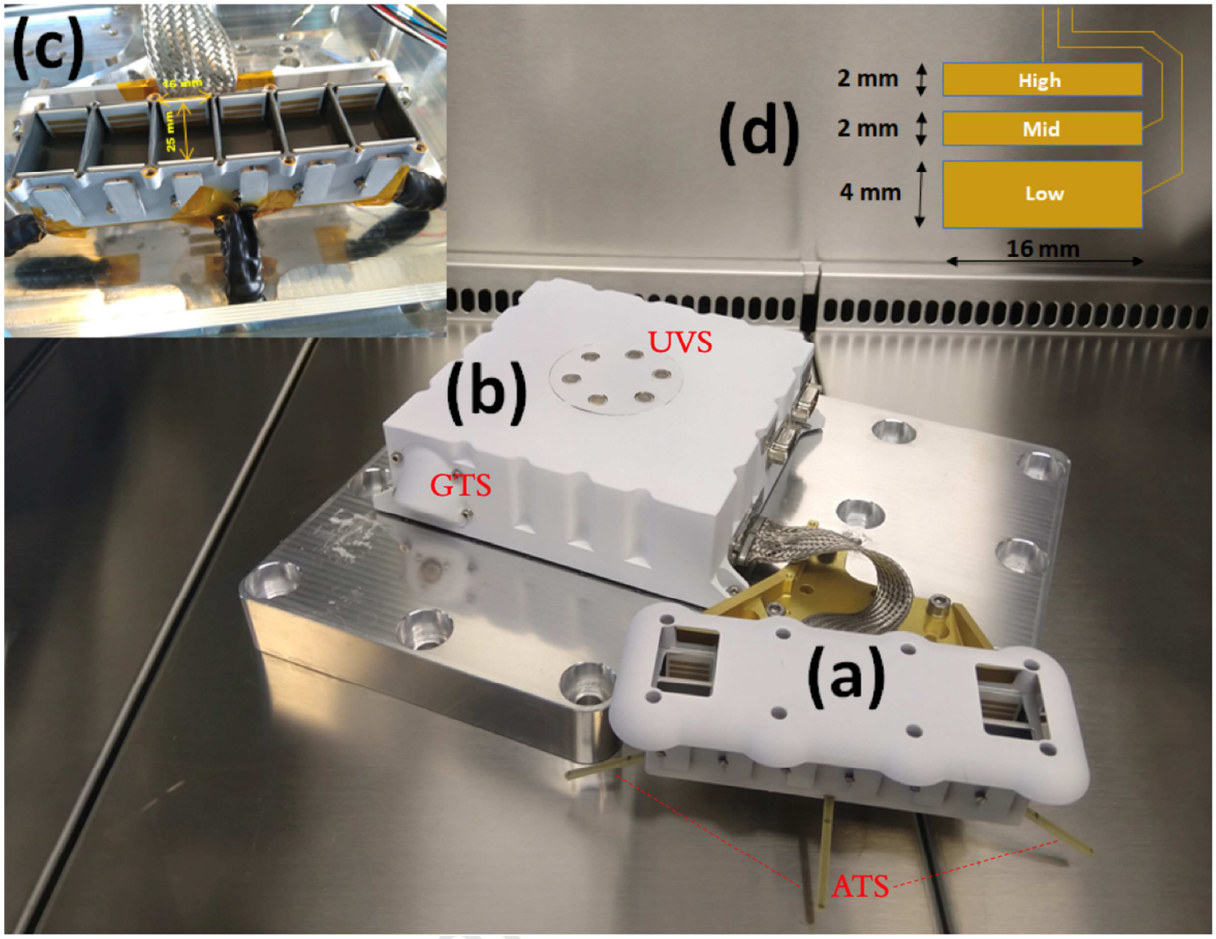

225

226

227 **Figure 1:** HABIT Flight Model (FM): (a) Container Unit (CU) with BOTTLE and the
228 three ATS, (b) Electronic Unit (EU) with the UVS and GTS, (c) Open view of the empty con-
229 tainers of BOTTLE with the golden electrodes, and (d) Electrode dimensions and separations.

230

231 The container Unit (CU) which includes the six containers of BOTTLE and the three Air
232 Temperature Sensors (ATS) will be exposed to the free flow of air, mounted on the edge of
233 the ExoMars SP. The Electronic Unit (EU) is mounted on top of the SP deck, with the ultra-
234 violet sensors (UVS) pointing to the sky, and the ground temperature sensor (GTS) pointing
235 to the side, with a clean field-of view, to monitor the temperature of the surface of the ground.
236 The UVS is located in the EU lid centre and it includes six different photodiodes embedded
237 within magnetic rings to deflect the trajectory of in-falling airborne dust and extend the life-

time of the sensors by keeping their field of view clean. The UVS has a free view of sky of 60° solid angle which make HABIT exposed to both direct sunlight and diffuse irradiance without any shielding. The GTS is located on the short edge of the instrument. This sensor is pointing toward the ground in an angle of 45°. The CU contains the six electric conductivity cells of BOTTLE and three ATS. Two cells are open and four are sealed with a High Efficiency Particle Air (HEPA) filter, with pore size 0.3 μm, and covered by a roof that allows the flow of air while preventing direct obstruction by dust. The filter has two purposes: it prevents inbound and outbound bioburden (organics or microbes) contamination and protects the salts from dust while allowing air to flow in. The two open cells are aimed at investigating the electrical conductivity of the martian air, as it changes throughout days and seasons depending on the amount of atmospheric water. Also, when airborne dust starts to accumulate at the bottom of these containers, the electrodes will provide a measurement of the conductivity of dust. The four central cells of BOTTLE are filled with four deliquescent salts that have been reported on Mars, and a super absorbent polymer that will form a hydrogel when the deliquescent salts absorb water. This hydrogel will keep the brine in a semi-solid state, avoiding capillarity of the pure liquid phase while supporting the capture of water and thus allowing to measure electrical conductivity. The two open air cells have two measuring electrodes, whereas the cells with the encapsulated products have three measuring electrodes. The quantity of products is chosen such that the dry product covers fully the lower electrode, allowing for expansions and contractions as the products absorb water, freeze or melt. When the salt turns into liquid brine the volume increases, and the mid electrode may also be in contact with the salt. The upper electrode is for control in case of inclination of the platform.

The data acquired by the sensors will be complemented with the timestamp of the acquisition moment and the platform inclination will be taken into account as ancillary data. This

ancillary information is needed to interpret the solar UV measurements, because the response of the sensors depends on the angle of incidence of the direct irradiance from the Sun, also the estimate of the total column of dust depends on the traversed slant path from the Sun to the platform. A set of engineering housekeeping temperature sensors monitors the temperature of the UVS, GTS and the EU and CU. The UVS and GTS temperature sensors are needed to apply the adequate calibration functions and retrieve the observable variables. Whereas the EU and CU temperature measurements are needed to activate the heaters.

The instrument shall operate autonomously at day- and night-time and communicate with the central computer once per sol. The regular, nominal, cadence of observation will be five minutes at the beginning of each hour, acquiring data at 1 Hz. The EU includes different electronic functions such as start-up heaters, power supply, data handling and sensitive analogue sensor circuits.

3. Air temperature and wind retrieval from the Air Temperature Sensors (ATS)

The HABIT Air Temperature Sensors (ATS) design, main working principles, and operation modes are illustrated in section 4.1. Also, the calibration procedure of the HABIT FM ATS is included in that section, together with results of the FM calibration campaign at Omnisys Instruments AB facilities. The ATS in HABIT is an evolved version of the REMS ATS currently operating on the surface of Mars on board the NASA Mars Science Laboratory/ Curiosity rover. In this section we summarize a novel wind retrieval method that is based on the analy-

sis of the heat-flux of the ATS. In section 4.2, we will present an example of the calibration of the ATS for wind retrieval under martian conditions, in the wind tunnel facility of Aarhus.

a. Design and operation of the ATS.

The near-surface air temperature changes mostly with the solar irradiance, varying about 90 K between the day and night following the diurnal thermal tide; and following a seasonal behaviour along the year, depending on the solar longitude. The temperature also affects the martian air density and it is important to describe the near surface heat-transfer processes. Furthermore, the temperature may show slow fluctuations in response to natural convection that takes place at the planetary boundary layer during the day; it may also show the temperature of air masses brought by wind from other locations, such as in the case of katabatic winds; and it may also vary rapidly in response to very quick phenomena, such as dust-devils. To monitor the air temperature in the vicinity of the platform, HABIT incorporates three ATS in three different orientations.

Figure 2 shows a detail view of ATS rod 1 mounted on the HABIT FM CU structure. Each ATS consist on three rods of length L = 3.6 cm made of FR4 material with three Pt1000 thermistors attached at three different positions, to measure the temperature profile along the rods. The temperatures recorded by each Pt1000 are expected to be thermally influenced by the conductive heat exchange between the rods and the HABIT structure, which is in turn thermally coupled to the SP. By monitoring these temperature profiles, the ATS can obtain an ambient temperature corresponding to the film temperature of the SP. The material of the rods has a low thermal conductivity, of k = 0.7 W/mK.

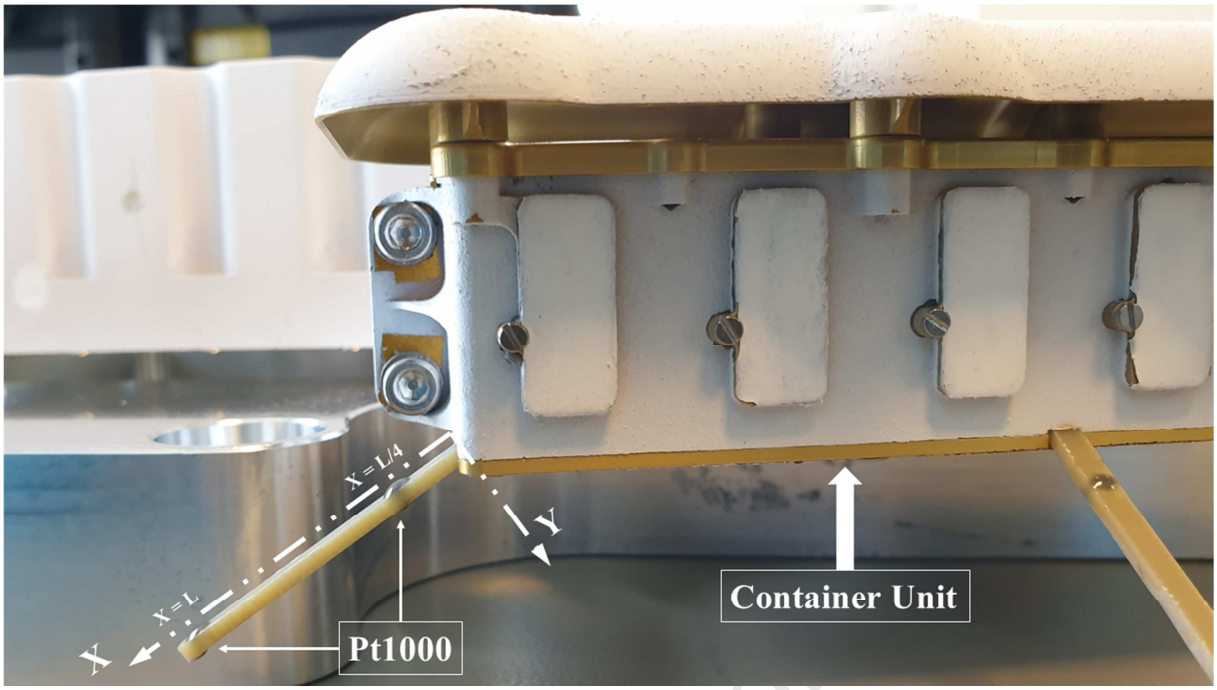

Figure 2: Detailed view of one of the ATS 1 attached to the side of the HABIT FM CU, and partial view of the frontal ATS. Three Pt1000 thermistors are located at x = 0, x = L/4 and x = L in order to record the temperature at the base, Tb, at the intermediate point, TLn, and at the tip of the rods, Ta, respectively. The Pt1000 at the base of the rod, x = 0, is not visible.

The air temperature acquisition performed by HABIT is similar to the REMS ATS recording (Gómez-Elvira, et al., 2012), and it is based on modelling the energy balance along a fin that is cooled by natural convection (Mueller & Abu-Mulaweh, 2006). Considering a local coordinate system at the ATS rods, where x = 0 is at the interface between the ATS rods and the CU wall (see Figure 2). Each rod has one thermistor at the tip (x = L) recording the temperature Ta, a second one at the base (x = 0) recording Tb, and a third one at an intermediate point, x = L/4, recording the temperature TLn. By assuming that the HABIT CU structure is in thermal equilibrium with the ambient, it is possible to express analytically the temperature distribution along each rod as a function of an average dimensionless variable $\overline{m}$, (here referred as the m-parameter), which is dependent on the thermal conductivity k, geometry, and average heat transfer coefficient $\bar{h}$ of the rods.

$$\theta(\chi) = \theta_b \frac{\cosh[\bar{m}(1-\chi)]}{\cosh(\bar{m})}, \quad (1)$$

$$\bar{m} = L\sqrt{\frac{\bar{h}A_s}{kA_c}} \ . \quad (2)$$

Here, $\theta = T - T_\infty$ is the excess temperature, $\theta_b = T_b - T_\infty$ the excess temperature at the base of the rod, and T_∞ the temperature outside the thermal boundary layer of the rod. The latter was assumed to be similar to the fluid temperature $T_\infty \sim T_f$. A_s and A_c represent the lateral and cross-section areas of the rods, respectively. It should be noted that the $\bar{h}$ coefficient collects the radiative and convective terms, $\bar{h}_c$ and $\bar{h}_r$, where constant emissivity, ε, and thermal conductivity have been assumed along the rods. The $\bar{h}$ coefficient is assumed uniform and equal to:

$$\bar{h} = \bar{h}_c + \bar{h}_r = \bar{h}_c + \varepsilon\sigma(T^2 + T_\infty^2)(T + T_\infty), \quad (3)$$

where σ is the Stefan-Boltzmann constant. By introducing the three temperature readings at each ATS rod in Equation (1), it is possible to establish a system of two equations with the average m-parameter, $\bar{m}$, and the fluid temperature, T_f, as unknowns:

$$\begin{cases} T_a - T_f = (T_b - T_f)\frac{1}{\cosh[\bar{m}]} \\ T_{Ln} - T_f = (T_b - T_f) \cdot \frac{\cosh\left[\bar{m}\cdot\left(1-\frac{1}{n}\right)\right]}{\cosh[\bar{m}]}. \end{cases} \quad (4)$$

This approach is implemented on REMS, to obtain T_f, by solving the system (4). HABIT is designed to replicate this working principle for the ExoMars SP (Soria-Salinas, et al., 2020a). As can be inferred when solving the system of equations (4), the fluid temperature T_f depends on the absolute temperatures provided by the thermistors, but $\bar{m}$, as seen on Equation (1), is only dependent on the temperature differences. The temperature readings need to be calibrated against a reference temperature probe to obtain the actual T_f.

The calibration of the thermistors was performed in a thermal vacuum chamber (TVAC) close to vacuum conditions. On Mars, because of the low atmospheric density, the dominant heat-exchange mechanism is radiative heat transfer, while on Earth, at ambient pressures, the higher density environment makes natural convection the dominant process. One of the calibrations was performed under vacuum conditions in order to reduce the influence of the atmosphere and correct for the self-heating contamination produced by the initiation of the instrument. Figure 3 shows the setup used for the HABIT flight model (FM) within the Omnisys Instruments AB TVAC chamber. The test was performed at ambient temperatures for 12 hours using a reference temperature probe HEL-705-T-0-12-00 with an accuracy of ± 0.8% (around ± 0.2°C at 25°C) at a pressure of $1 \cdot 10^{-6}$ bar.

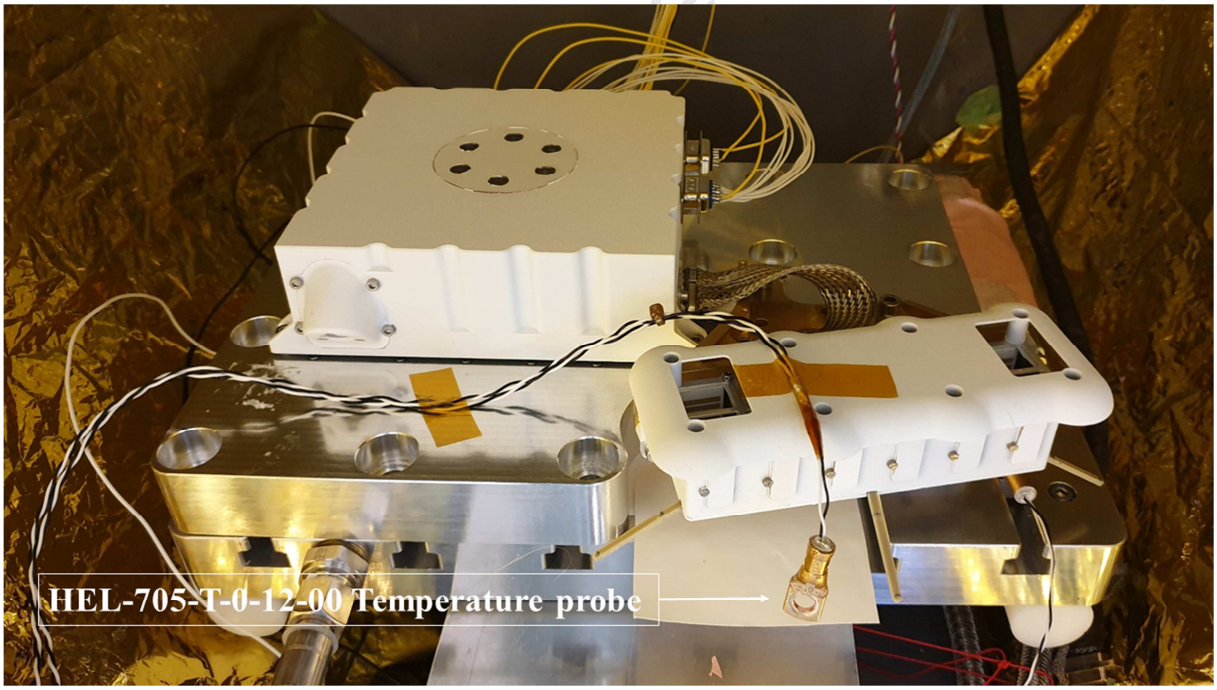

Figure 3: Setup for the HABIT flight model (FM) ATS calibration under low-pressure conditions, $P = 1 \cdot 10^{-6}$ bar, and ambient temperature, $T = 25℃$, in the Omnisys Instruments AB TVAC. The reference temperature probe was a HEL-705-T-0-12-00 with an accuracy of ± 0.8% and the pressure monitored by a 'Leybold TR-211 Thermovac Pirani Vacuum Sensor'.

The pressure at the chamber was monitored by a 'Leybold TR-211 Thermovac Pirani Vacuum Sensor' and maintained to $1 \cdot 10^{-6}$ bar, and the reference temperature was measured by a 'HEL-705-T-0-12-00' probe with an accuracy of ± 0.8%. The probe was fixed close to the ATS rods in order to expose the sensor to the most similar radiative environment possible. In this test, all the nine temperatures provided by the Pt1000 were fitted to the reference temperature. An average offset with respect to the reference temperature was calculated using the measurements of each sensor. This allowed us to remove the initial temperature profiles originated from the self-heating of the instrument when switched-on. The instrument was configured to perform an extended acquisition of 3 hours at 1 Hz for the calibration. The differences were corrected with the averaged offsets that each thermistor presented during the central hour of the extended acquisition period. The results of the calibration can be observed in Figure 4.

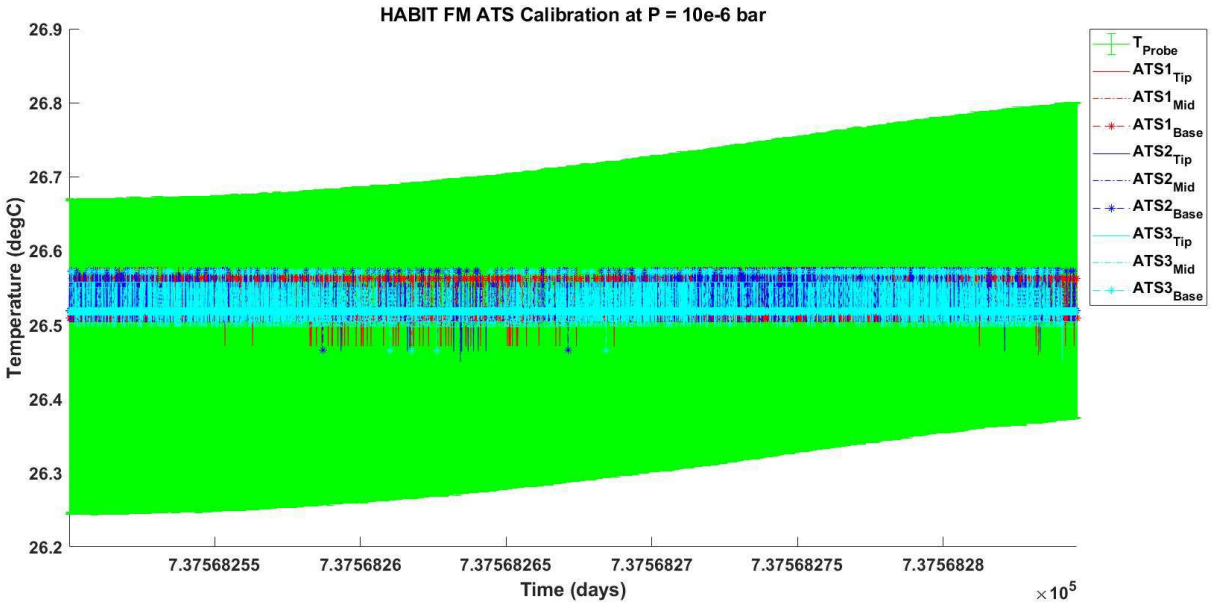

Figure 4: Results of the ATS calibration at $P = 1 \cdot 10^{-6}$ bar and $T = 25$℃. conditions, including the temperature probe HEL-705-T-0-12-00 absolute error of ±0.8%, during the central hour of a 3-h extended acquisition.

As it is shown in Figure 4, during the ATS calibration the reference probe presented an oscillation of ±0.1°C limited by the capability of the thermal plate that was set to maintain the HABIT structure temperature at 25 °C. However, it must be noted that the overall accuracy of the probe for the temperatures tested is around ±0.2 °C, as indicated in Figure 4 by the error bar, which makes this variation negligible. As can be observed in the figure, the stability of the Pt1000 readings in this hour of extended acquisition are always contained within the boundaries of the errors of the reference temperature probe. As a result of this calibration, the Pt1000 measurements at each rod are now capable of measuring temperatures at a resolution of 0.05°C and with an accuracy of ±0.2 °C.

b. Wind retrieval from the ATS heat-flux analysis.

The recent results from the analysis of REMS ATS and WS dataset on Mars suggested the possibility of using the REMS ATS temperature data to provide the MSL mission with wind speed (Soria-Salinas, et al., 2020a). The main working principle of this wind retrieval method is the use of the estimated average m-parameter at each rod, $\bar{m}$. This parameter was calculated in the original fluid temperature retrieval performed by REMS, but it was neither stored nor further processed. According to its definition, the m-parameter is correlated with the wind speed through the average convective heat transfer term, $\bar{h}_c$, included in the average heat transfer coefficient, $\bar{h} = \bar{h}_c + \bar{h}_r$ (see equation (2)). In addition, the $\bar{h}_c$ coefficient of each rod is dependent on natural and forced convection; that is, on the relative speed of the airflow that surrounds the ATS rods. Thus, if the correlation between the $\bar{h}_c$ coefficient and cooling airflow relative speed around each rod was modelled, wind speed could be retrieved, in first ap-

proach, from the estimated m-parameters. The proposed wind-retrieval method is thus based on modelling the forced convection on the ATS rods (Soria-Salinas, et al., 2020a). This work shows that this retrieval technique, when applied to REMS ATS data, matched the REMS WS wind speed values (allowing for WS errors of 20%, the error of the sensor according to Gomez-Elvira, J., 2013 a,b,c) up to ~77% of the time when the incident horizontal wind field direction was $\alpha \in [12.95°, 107.05°]$ (α is defined as the horizontal angle clockwise from REMS Boom 2 relative to Boom 1, see Soria-Salinas, et al. 2020a).

Because the HABIT ATS design is based on REMS ATS, the wind retrieval developed for the REMS dataset is also applicable to HABIT. In this case a set of calibration experiments are needed to convert the derived heat-transfer to the corresponding wind speed and to calibrate the emissivity to thermal conductivity ratio. A wind tunnel campaign was performed in the Aarhus Wind Tunnel Simulator (AWTS), Aahrus University, Denmark, with the main goal of assessing the overall error of the wind retrieval concept when applied to the HABIT EQM ATS temperature measurements. This facility has been frequently used for the testing of space hardware for Mars (Holstein-Rathlou, et al. 2010). Two tests were performed so that the ATS rods were exposed to a normal airflow. These tests were also used to verify the thermal conductivity of the HABIT ATS rods after the Pt1000 thermistors and associated printed circuity (Soria-Salinas, et al. 2020b). The tunnel consists on a TVAC that possess an electric motor (Danfos VLT5001) that moves an internal fan magnetically coupled. This fan creates a close circuit of low-pressure air that can replicate typical low-speed winds on the surface of Mars. The cylindrical tunnel is around 8 m x 2.5 m, although the effective testing area, far from wall interference, is about 0.4 m in diameter (Merrison, et al., 2008). Wind speeds up to ~16 m/s could be simulated within the tunnel, although beyond ~ 8 m/s the friction of the recirculating air artificially overheats the flow (Soria-Salinas, et al. 2020b).

Figure 5 shows the setup for the two tests performed within the AWTS and the reference system considered. Test 1 simulated front winds ($\alpha = 0°$), where the airflow is perpendicular to both ATS rod 1 and ATS rod 3. Test 2 simulated lateral winds ($\alpha = -90°$); that is, airflows perpendicular to the ATS rod 2. The range of wind speeds tested in the tunnel was limited to $V \lesssim 12$ m/s because of excessive overheating of the airflow observed during the operations.

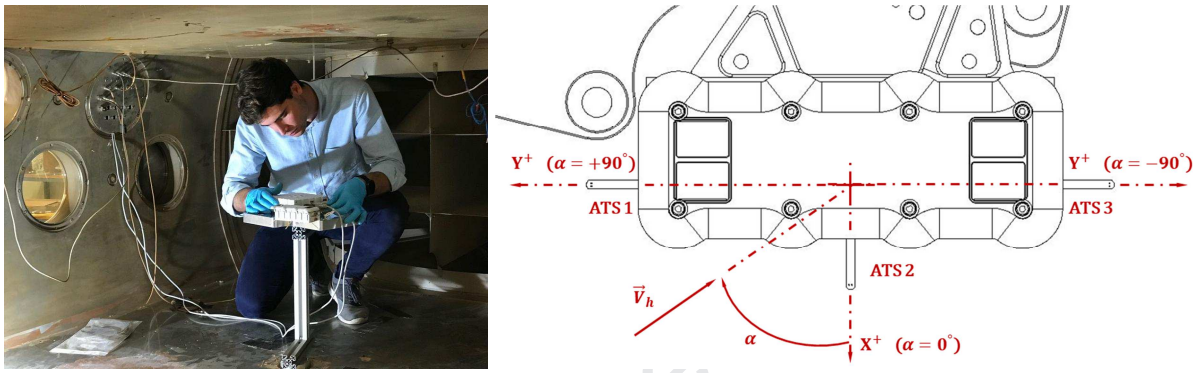

Figure 5: (Left) HABIT EQM setup within the AWTS. The instrument is attached to an aluminium mast through a thick aluminium plate. The mast could rotate in the horizontal plane 360° with respect to the centre of the EQM CU. The tunnel fan that suctions the air towards the EQM is visible behind the setup. (Right) HABIT CU top view including the reference system used for the tested wind orientation. Test 1 simulated front winds ($\alpha = 0°$) and Test 2 simulated lateral winds ($\alpha = -90°$).

As it was mentioned earlier, the HABIT wind speed retrieval method relies on the modelling of forced convection on the ATS rods. The main purpose is then to obtain an analytical expression that correlates the averaged convective heat transfer coefficient at each rod, $\bar{h}_c$, estimated from $\bar{m}$, with the local wind speed. This was performed through the average Nusselt number,$\bar{N}_u$, defined as the ratio of convective to conductive heat transfer terms within the boundary layer developed around the ATS rods, $\bar{N}_u = \bar{h}_c \cdot L_c/k$. Here, L_c represents the characteristic length.

The rectangular-based ATS rods were assumed to be cylinders and several empirical formulations of $\bar{N}_u$ for normal cross-flow were assessed (Fand and Keswani, 1972; McAdams, 1954; Perkins and Leppert, 1964; Van Der Hegge Zijnen, 1956). These $\bar{N}_u$ models were developed for similar fluid flow regimes to the expected low-density airflows on the surface of Mars and for the L_c of the heat transfer problem on the ATS rods; in this case $L_c \sim$ diameter of the cylinders. As a result, by comparing the $\bar{h}_c$ coefficient estimated from $\bar{m}$ with the $\bar{h}_c$ resulting from the averaged Nusselt number model at each rod, it is possible to obtain the wind speed. Equation (5) summarizes the analytical expression developed for the wind speed retrieval, whose solution provides wind speed from the estimated $\bar{m}$ values.

$$\bar{h}_c = \frac{\bar{m}^2 \cdot K \cdot a \cdot b}{L^2 \cdot 2 \cdot (a+b)} - \sigma\varepsilon(T_s^2 + T_\infty^2)(T_s + T_\infty) = \frac{k}{L_c} \cdot \bar{N}_u. \quad (5)$$

Here, $a = 2\,mm$ and $b = 3\,mm$ correspond to the sides of the rectangular cross-section of each ATS rod, T_∞ is the temperature of the fluid Tf which is retrieved through equation (4) and Ts the temperature of the ATS surface which is calculated from the average of the temperatures provided by the three ATS thermistors. From the wind tunnel tests performed in the AWTS, and according to the concussions from the application of the retrieval concept to the REMS temperature data when compared to the REMS WS values (Soria-Salinas, et al., 2019a), the average Nusselt number model developed by S. Whitaker (Van Der Hegge Zijnen, 1956) was selected for the ATS rods (see equation (6)).

$$\bar{N}_u = \left(0.4 \cdot Re^{0.5} + 0.06 \cdot Re^{2/3}\right) \cdot Pr^{0.4} \cdot \left(\mu_f/\mu_s\right)^{0.25}. \quad (6)$$

In equation (6), $Re = \rho U_\infty L_c/\mu$ is the Reynolds number, which represents the ratio between the viscous and convective terms of a fluid flow of density ρ with unperturbed wind speed U_∞, which for our tests is V_{Tunnel}, and dynamic viscosity μ around the rods of diameter L_c. Pr $= \mu \cdot C_p/k$ is the Prandtl number, that represents the ratio between the momentum diffu-

sivity and thermal diffusivity within a fluid flow of specific heat at a constant pressure C_p and thermal conductivity k. μ_f and μ_s correspond to the dynamic viscosity evaluated at the fluid temperature, T_f, and at the averaged surface temperature of the rods, T_s, respectively.

The final accuracy of the ATS wind speed retrieval was set based on the comparison with the wind tunnel reference values. The latter were obtained after the calibration of the correlation between the fan revolutions per minute, and the measurements provided by a commercial Dantec laser Doppler anemometer; the nominal errors at the testing area for the selected range of wind speed is $\pm$0.3 m/s (Merrison, et al., 2008).

Although both ATS 1 and ATS 3 were equally exposed to the same free stream, the experiments suggested that the aluminium plate to which the HABIT CU was attached locally modified the horizontal velocity field in the vicinity of the ATS rod 1; that is, ATS rod 1 was too close to the plate and the perturbation introduced in the flow by the latter modified the airflow upstream. As a result, no reference value of the actual wind speed sensed by the ATS rod 1 was available to be compared with the retrieval prediction. When compared to the free stream speed values, the maximum error observed in the ATS rod 1 retrieval, assuming the Whitaker approach, was 0.81 m/s for $V_{Tunnel} \in [0,10]$ m/s. ATS 3, on the contrary, demonstrated to be sufficiently separated from the plate and this hypothetical perturbation into the ATS rod 3 surrounding airflow was not observed, providing a maximum wind speed retrieval error of 0.28 m/s with respect to the reference values for $V_{Tunnel} \in [0,10]$ m/s. It should be noted that both the shape of the aluminium plate and CU relative orientation to the platform are not similar to the final configuration on board the SP, both ATS1 and ATS3 are similarly distant from the SP. However, for calibration purposes we shall use the tests of the ATS that is less perturbed by its holding structure. Then on Mars, the three ATS will provide the wind measurement at the place where they are installed, namely this local wind may be significantly different from

the free flow of air on Mars. This contamination is unavoidable for any instrumentation mounted on a landed spacecraft on Mars. As a result, from the AWTS analysis an error of 0.81 m/s was assumed for both sensors to predict possible unknown interference on the retrieval of frontal winds (Soria-Salinas, et al., 2020b).

Results from Test 2, where the CU was exposed to lateral winds ($\alpha = -90°$), demonstrated the ATS 2 wind speed prediction capabilities, for the Whitaker approach, with an maximum error of 0.29 m/s for $V_{Tunnel} \in [0,6]$ m/s; that is, comparable to the wind tunnel wind speed reference probe error. However, ATS rod 2 results exposed a limitation in the wind speed retrieval for $V_{Tunnel} \in [6,10]$ m/s inherent to the instrument structural design. The results suggested that, for horizontal lateral winds, the viscous boundary layer developed along rectangular shape of the CU structure could present separation bubbles along its entire lateral surface for wind speeds > 5.5 m/s. Okajima (1990) predicted this point for a Reynolds number, based on the length of the larger side of the CU ($L_c = A$), at $Re_A \sim 200$, which agrees with the Reynolds at $V_{Tunnel} = 5.5$ m/s; that is, $Re_A = 193$ (Soria-Salinas, et al., 2020b).

Figure 6 shows as an example the retrieval output when applied to ATS rod 3 under front winds in Test 1 ($\alpha = 0°$).

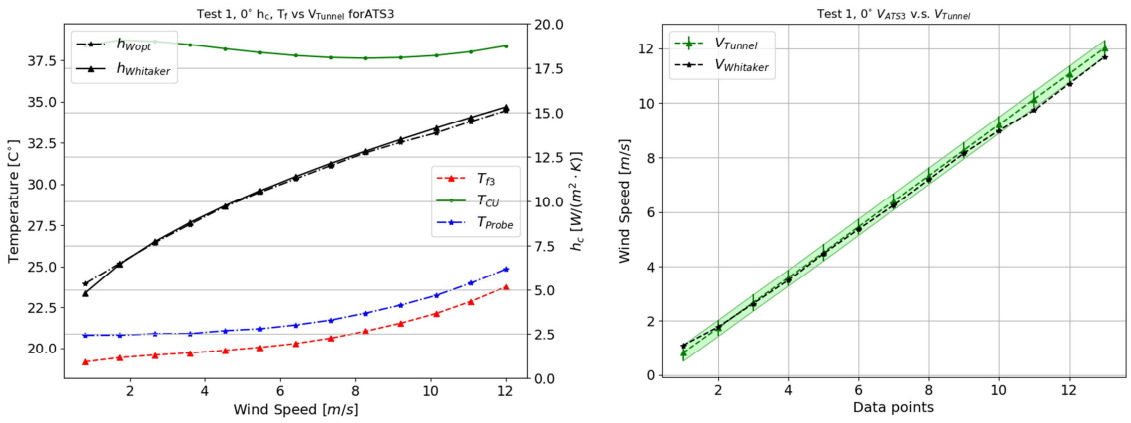

Figure 6: (Left) Comparison of the evolution of the average convective heat transfer coefficient estimated from $\overline{m}$, $\bar{h}_{Wopt}$ (assuming the Whitaker approach for the $\overline{N}_u$ modelling), with respect to the theoretical coefficient associated to the free stream wind speeds, $\bar{h}_{Whitaker}$, on the ATS rod 3. The estimated fluid temperature, T_{f3}, as well as the temperatures from the CU Pt1000, T_{CU}, and the tunnel,T_{Probe} (which is in a distant position in the tunnel), are also included. (Right) Comparison of the wind speed prediction performed by the ATS rod 3 with the free stream wind speed values. The errors associated to the wind speed reference estimation of $\pm$0.3 m/s have been included.

As can be seen on Figure 6 (left), the average convective heat transfer coefficient estimated from $\overline{m}$, $\bar{h}_{Wopt}$, fairly match the theoretical predictions of this coefficient, $\bar{h}_{Whitaker}$, when the wind speed measured by the tunnel probe, V_{Tunnel}, is used for its calculation (instead of $\overline{m}$). Also, the overheating of the airflow because of the friction of the flow with the inner tunnel walls can be observed on the temperature evolution of the tunnel temperature probe, T_{Probe}. Figure 6 (right) shows the comparison between the wind speed retrieval and the free stream wind speed values tested. Here, the tunnel wind speed reference error of $\pm$0.3 m/s has been included. Each wind speed value tested was kept constant for 10 min, and both the reference and retrieval wind speed values were averaged for this period.

In summary, the wind tunnel campaign performed in the AWTS allowed us to assess the capabilities and main limitations of the HABIT ATS wind retrieval for frontal and lateral winds. The formers are expected to be retrieved with a maximum error of 0.81 m/s from ATS 1 and ATS 3 for horizontal wind speeds $V \in [0,6]$ m/s, assuming some perturbation from the ExoMars SP. The latter, with a maximum error of 0.29 m/s from ATS 2 for horizontal wind speeds $V \in [0,6]$ m/s; the platform is not expected to interfere in the airflow around ATS rod 2 in this case. Future wind tunnel studies are planned to investigate the time response sensitiv-

ity to varying winds, the role of the temperature and the possibility to extract information about the angle of incidence of the wind.

4. Ground Temperature Sensor (GTS)

The HABIT Ground Temperature Sensor (GTS) monitors the temperature at a single spot of the surface at the landing site. The GTS is a light weight, low power, and low-cost pyrometer that will measure the soil kinematic temperature of the martian surface during the nominal mission lifetime of one Earth year. It benefits from a simple design with no moving parts and its fixed pointing to the martian surface at an angle of 45°. The sensor acquires its heritage from the Rover Environmental Monitoring Station (REMS) Ground Temperature Sensor (GTS), an instrument aboard the NASA's Mars Science Laboratory (Gomez-Elvira et al., 2012; Gomez-Elvira et al. 2014). Figure 7 shows the Engineering Qualification Model (EQM) of HABIT, including GTS as a part of the Electronics Unit (EU). In this section, we describe the design of GTS, the energy balance model and the associated calibration with the Engineering Qualification Model (EQM) and the Flight Model (FM).

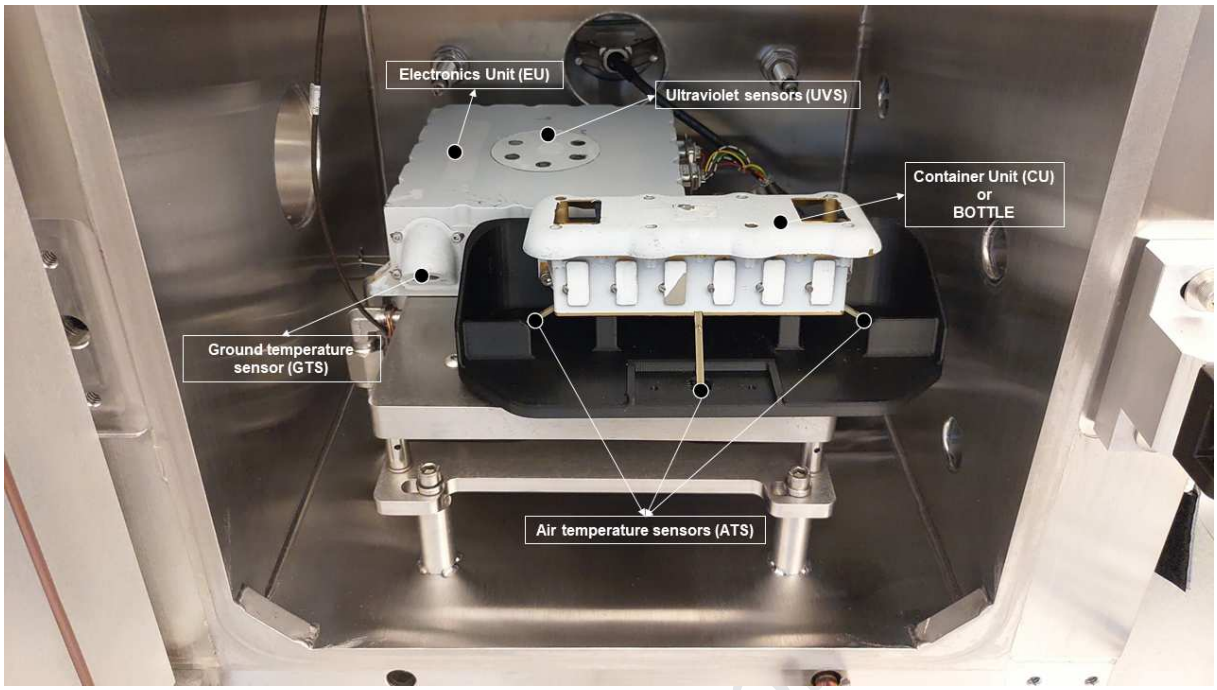

Figure 7: Image of the HABIT instrument Engineering Qualification Model (EQM) in the SpaceQ chamber highlighting the Container Unit (CU), Electronic Unit (EU) with Ground Temperature Sensor (GTS) and other sensors.

4.1 Design and operation

The core of the GTS is an 8-14µm wavelength band sensitive infrared thermopile (Figure 8), which depending on the total energy influx from its field of view, converts this to a corresponding voltage output.

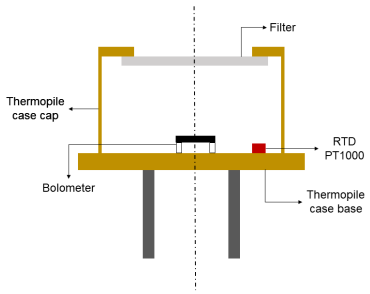

Figure 8: Schematic representation of a cross-section of a thermopile and its components.

The sensing area of the thermopile that receives the energy from its field-of-view and converts it to a voltage is the bolometer. The response depends on the difference in temperature with the thermopile case base (cb) as measured with the help of a Pt1000 temperature sensor. The incoming energy passes through an 8-14μm band-pass filter to measure temperatures in a range specific to the Mars. The blackbody temperature for a peak wavelength can be calculated using the Wien's displacement law as shown in equation (7).

$$\lambda_{max} = \frac{2898}{T}\ (\mu m) \qquad (7)$$

The thermopile with its 8-14μm band-pass filter is sensitive to measure a temperature range between -66.17 °C and 89.07 °C.

4.2 Measurements and calibration

The GTS measures the thermopile case base (cb) temperature and the thermopile output as ADC counts. HABIT uses a 12-bit ADC (4096 step resolution) with a reference voltage (V_{ref}) of 4.096 V. The amplifier gain (A_v) is set to 201 in order to read the output signal, since the output voltage produced by the thermopile is marginally smaller that the reference voltage. The thermopile output voltage ($V_{thermopile}$) can be calculated using equation (8).

$$\mathrm{V_{thermopile}} = \frac{1}{A_v} * \left(\frac{ADC\ counts * \mathrm{V}_{ref}}{\mathrm{ADC\ resolution}}\right) = ADC\ Counts * \left(\frac{100}{201}\right)(\mu V) \qquad (8)$$

The resultant voltage output is a function of the difference in temperature between the thermopile case base (cb) and the bolometer (s) as expressed in equation (9).

$$\mathrm{V_{thermopile}} = f(T_{cb})(T_s - T_{cb}) \qquad (9)$$

where, T_{cb} is the temperature of the thermopile case base and T_s is the temperature of the bolometer.

For the IPHT TS-100 thermopile used in the GTS, the relationship is provided by the manufacturer as in equation (10).

$$f(T_{cb}) = -88.86 * 10^{-4} + 3.057 * 10^{-4}.T_{cb} - 0.01526 * 10^{-4}.T_{cb}^2 + 3.366 * 10^{-9}.T_{cb}^3 - 2.788 * 10^{-12}.T_{cb}^4 \quad (10)$$

For a set of 100 thermocouples connected in series in the thermopile, equation (10) is modified to equation (11)

$$V_{\text{thermopile}} = 100.f(T_{cb})(T_s - T_{cb}). \quad (11)$$

4.2.1 Energy balance model

In a non-contact measuring instrumentation like the thermopile, the energy flux contributing to the temperature measurement could be of conductive, convective and radiative nature as shown in Figure 9.

The energy balance equation (Gómez-Elvira et al., 2012, Sebastian et al. 2010) is expressed in equation (12):

$$P_{R,g-s} + P_{R,f-s} + P_{R,cc-s} + P_{R,cb-s} + P_{C,cb-s} = 0 \quad (12)$$

where, P – Energy

R – Radiation

C – Conduction

g – Ground

f – Filter

cc – Thermopile case cap

cb – Thermopile case base

s – Bolometer

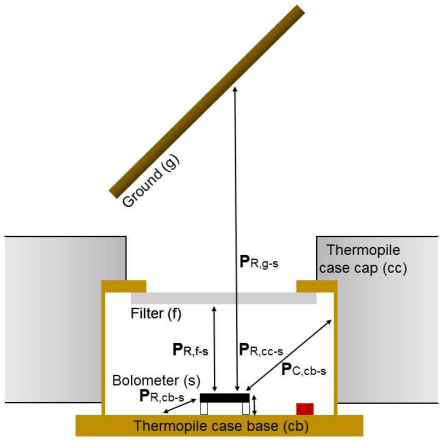

Figure 9: Graphical representation of the conductive, convective and radiative energy fluxes associated within the thermopile and with the external environment. The black arrows show the interaction between the different components of the thermopile with the subscripts depicting if the nature of the energy flux is conductive, convective or radiative in nature.

Considering constants K_1, K_2, and K_3, each representing the relative weight of different energy transfer processes, and assuming filter temperature, T_f and the thermopile case cap temperature, T_{cc} are the same as the thermopile case base temperature, T_{cb}, since there are in contact with each other, the simplified energy balance equation obtained is as shown in equation (13).

$$K_1\left(\Phi_g^I - \Phi_s^I\right) + K_1(\Phi_{cc}^O - \Phi_s^O) + K_2(\Phi_{cc}^T - \Phi_s^T) + K_3(T_{cb} - T_s) = 0 \quad (13)$$

where, Φ - Heat flux

I – Heat flux of radiation passing through filter (wavelength restricted)

O - Heat flux radiation not passing through filter

T - Heat flux of radiation in total spectrum (all wavelengths)

The different heat flux terms are calculated using Planck's law as shown in equations (14) to (19).

$$\Phi_g^I = \varepsilon_g \int_{\lambda_a}^{\lambda_b} T_f(\lambda) \frac{2hc^2}{\lambda^5\left(e^{hc/\lambda k_B T_g} - 1\right)} d\lambda \quad (14)$$

$$\Phi_{cc}^T = \int_0^{\infty} \frac{2hc^2}{\lambda^5\left(e^{hc/\lambda k_B T_{cc}} - 1\right)} d\lambda \quad (15)$$

$$\Phi_{cc}^I = \int_{\lambda_a}^{\lambda_b} T_f(\lambda) \frac{2hc^2}{\lambda^5\left(e^{hc/\lambda k_B T_{cc}} - 1\right)} d\lambda \quad (16)$$

$$\Phi_s^T = \int_0^{\infty} \frac{2hc^2}{\lambda^5\left(e^{hc/\lambda k_B T_s} - 1\right)} d\lambda \quad (17)$$

$$\Phi_s^I = \int_{\lambda_a}^{\lambda_b} T_f(\lambda) \frac{2hc^2}{\lambda^5\left(e^{hc/\lambda k_B T_s} - 1\right)} d\lambda \quad (18)$$

$$\Phi_{cc}^O = \Phi_{cc}^T - \Phi_{cc}^I \qquad \Phi_s^O = \Phi_s^T - \Phi_s^I \quad (19)$$

where, α_s – Bolometer absorptivity = 1

ε_g – Ground emissivity

ε_{cc} – Thermopile can cap emissivity = 1

ε_{cb} – Thermopile can base emissivity = 1

ε_s – Bolometer emissivity = 1

$T_f(\lambda)$ – Filter transmittance = 0.754

$\rho_f(\lambda)$ – Filter reflectance = 0

T_g – Ground temperature

T_f – Filter temperature

T_{cc} – Thermopile case cap temperature

T_{cb} – Thermopile case base temperature

T_s – Bolometer temperature

$T_f = T_{cc} = T_{cb}$

h = Planck's constant

c = Speed of light = 3 x 10^8 m/s

k_B = Boltzmann constant

λ_a = Minimum limit of the wavelength band of the thermopile filter

λ_b = Maximum limit of the wavelength band of the thermopile filter

4.2.2 Thermopile output voltage vs temperature

The purpose of calibration of the GTS was to determine the calibration constants in the energy balance equation and represent the output voltage produced by the thermopile to the brightness temperature of the target area in its field-of-view. We used a blackbody calibration source with emissivity (ε) equal to1 to establish this relationship. The calibration constants and the resultant energy balance equation obtained were used for the accurate conversion of

the thermopile output voltage to the target temperature assuming the emissivity of the martian surface from literature. The calibration procedure of the GTS consisted of three different blackbody targets: 1) Blackbody calibration source and controller (LumaSense Technologies M315X4-HT, Exit port: 101 mm X 101 mm) for ambient laboratory temperature experiments; 2) Peltier controlled thermographic paint coated aluminum plate for colder temperatures inside the climate chamber; and 3) Thermographic paint coated aluminum plate inside the SpaceQ Mars simulation chamber (an environment simulating facility designed and built for HABIT validation and calibration) at martian temperature, pressure and carbon-dioxide atmosphere (Vakkada Ramachandran et al., 2019). A MELEXIS MLX90614 infrared thermometer (with a temperature measurement range of -70 °C to 380 °C and a measurement accuracy and resolution of 0.5 °C and 0.02 °C respectively) was used as a reference for this application.

This experiment was conducted in three parts: i) under laboratory ambient, with blackbody temperatures between 25°C and 73 °C using LumaSense Technologies blackbody calibration source (see Figure 10); and ii) under martian temperatures in a climate chamber, with blackbody temperatures between 10°C and -50°C using the peltier controlled blackbody source (100 mm x 100 mm aluminium target coated with LabIR thermographic paint, normal emissivity of 0.92 for 8-14 μm band, see Figure 11); iii) under martian conditions of temperature, pressure and carbon-dioxide atmosphere in a simulation chamber, with blackbody temperatures between 10°C and -50°C with 10 °C interval using the thermographic paint coated aluminium plate with paint properties same as (ii), see Figure 12, attached to the liquid nitrogen cooled working table of the chamber. All the experiments were conducted in an ISO Class 7 clean room with HABIT EQM.

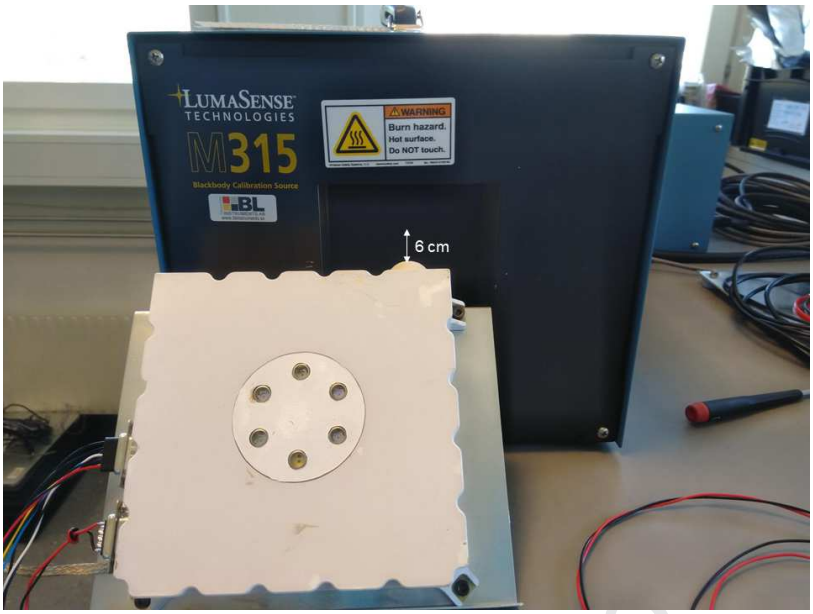

694

695 **Figure 10:** Experimental setup of the GTS mounted against the LumaSense Technologies
696 blackbody calibration source where the distance between the blackbody source and the GTS
697 is maintained at 6 cm.

698

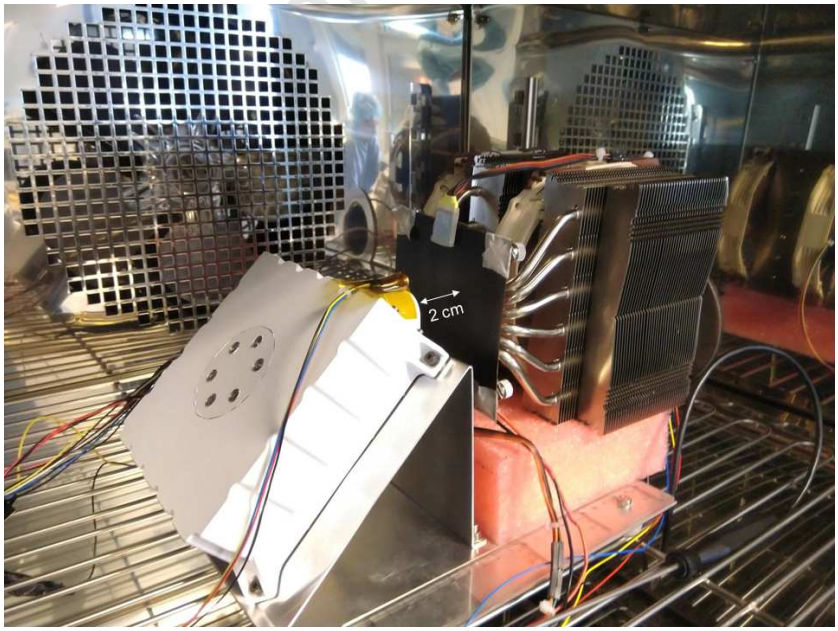

699

700 **Figure 11:** Experimental setup of the GTS against the Peltier-controlled thermographic paint
701 coated aluminium plate inside the climate chamber where the distance between the blackbody
702 source and the GTS is maintained at 2 cm.

703

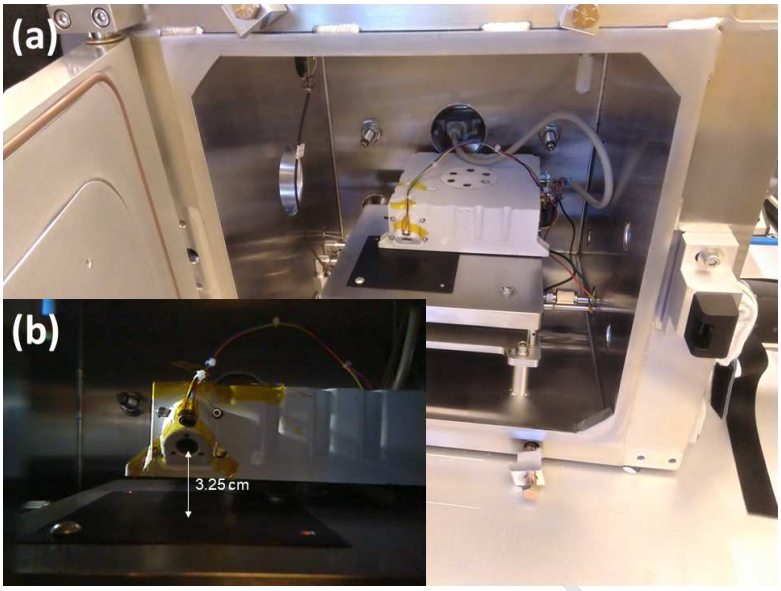

Figure 12: Experimental setup of the GTS against the thermographic paint coated aluminium plate inside the Mars simulation chamber where the GTS is maintained at a slant distance of 3.25 cm and pointed at an angle of 45°, representative of the operational scenario on Mars.

All the experiments were performed by maintaining a blackbody temperature between 73 °C and -50 °C, decreasing the temperature at 10 °C intervals while the ambient temperature was maintained relatively constant. For the experiment under martian conditions, an insulating spacer was used to isolate the Electronics Unit (EU) from the cold working table. The response of the thermopile was recorded for 100 data points at a frequency of 1000 ms.

The different distance between the GTS and the blackbody calibration source for each of the experimental setup (6 cm for LumaSense Technologies blackbody calibration source, 2 cm for peltier controlled for thermographic paint coated aluminum plate, and 3.25 cm for thermographic paint coated aluminum plate inside the SpaceQ Mars simulation chamber) was maintained such that the oval footprint of the thermopile's field-of-view was covering only the calibration target of the blackbody. Hence, the difference in distances does not affect the

accurate retrieval of the target temperature but rather provide an average brightness temperature from the area of coverage in the field-of-view of the thermopile. During HABIT deployment on Mars the distance between the GTS and the martian surface will be of 1.5 m. Since the temperature is computed from the overall radiation within the field-of-view, the same calibration can be used without any modification for its use on Mars.

4.2.3 Ground temperature calculation

From the energy balance equation (12) and adding radiation from blackbody reflections $\Phi_{reflection}$, we obtain equation (20):

$$K_1\left(\Phi_g^I + \Phi_{reflection} - \Phi_s^I\right) + K_1(\Phi_{cc}^O - \Phi_s^O) + K_2(\Phi_{cc}^T - \Phi_s^T) + K_3(T_{cb} - T_s) = 0 \quad (20)$$

For this calibration, all the data points from ambient laboratory tests with the Lumasense blackbody calibration source, the martian temperature tests in a climate chamber and the martian condition tests inside the SpaceQ Mars simulation chamber were used.

Solving this equation for pairs of blackbody temperatures,

$$K_1\left(\Phi_{g1}^I + \Phi_{reflection} - \Phi_{s1}^I\right) + K_1(\Phi_{cc1}^O - \Phi_{s1}^O) + K_2(\Phi_{cc1}^T - \Phi_{s1}^T) + K_3(T_{cb1} - T_{s1}) = 0$$

$$K_1\left(\Phi_{g2}^I + \Phi_{reflection} - \Phi_{s2}^I\right) + K_1(\Phi_{cc2}^O - \Phi_{s2}^O) + K_2(\Phi_{cc2}^T - \Phi_{s2}^T) + K_3(T_{cb2} - T_{s2}) = 0$$

$$K_1\left(\Phi_{g1}^I - \Phi_{g2}^I - \Phi_{s1}^I + \Phi_{s2}^I\right) + K_1(\Phi_{cc1}^O - \Phi_{cc2}^O - \Phi_{s1}^O + \Phi_{s2}^O) + K_2(\Phi_{cc1}^T - \Phi_{cc2}^T - \Phi_{s1}^T + \Phi_{s2}^T) + K_3(T_{cb1} - T_{cb2} - T_{s1} + T_{s2}) = 0 \quad (21)$$

K_1(=1), K_2, and K_3 are achieved from equation (21) using linear least square algorithm.

$[K_1\ K_2\ K_3]$ = [1 113.4336 -7462.499]

Using the constants K_1, K_2, and K_3 in equation (13), the ground heat flux term, Φ_g^I can be computed, as shown in Figure 13, for the measured blackbody temperatures.

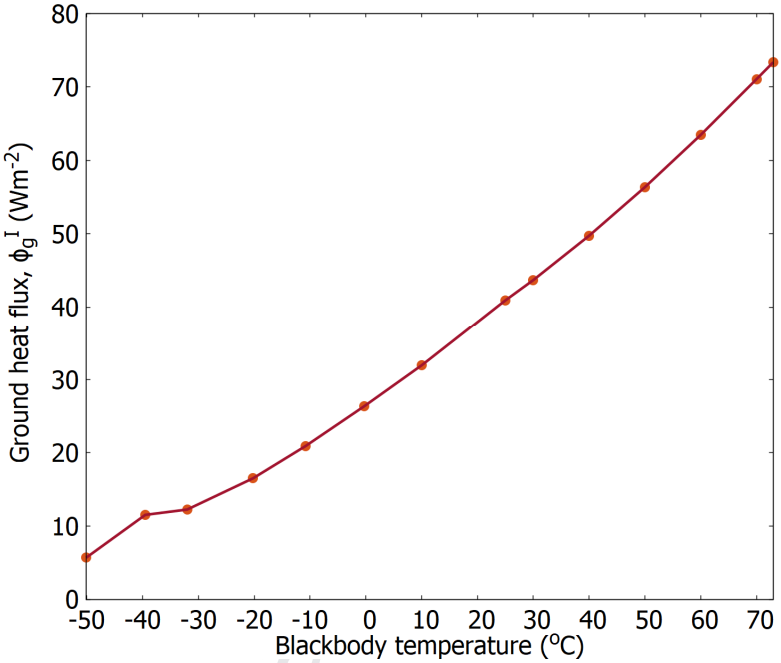

Figure 13: Computed ground heat flux values for the corresponding blackbody target temperatures based on equation (7).

The target temperature, T_g can then be calculated from the resultant ground heat flux using a 3rd order polynomial least square fit as expressed in equation (22).

$$T_g = 9.235e^{-05} . {\Phi_g^I}^3 - 0.0103. {\Phi_g^I}^2 + 1.8493. \Phi_g^I + 285.3986 \qquad (22)$$

The retrieved target temperature is the brightness temperature considering the blackbody with an emissivity, $\varepsilon = 1$. For martian surfaces where $\varepsilon \neq 1$, the assumed emissivity from the literature can substituted to recalculate the Φ_g^I term in equation (14) to retrieve the soil kinematic temperature on Mars.

763

764 **5.3 GTS performance**

765 The purpose of this experiment was to verify the overall performance of the GTS thermopile
766 response after obtaining the calibration constants from the tests described in section 5.2.2.
767 This experiment used the same setup of the LumaSense Technologies blackbody source and
768 the HABIT EQM but was performed as a continuous single sweep in the blackbody tempera-
769 tures from 73 °C to 40 °C including the transitions between temperatures. The experiment
770 was also conducted in an ISO Class 7 clean room with GTS thermopile at ambient tempera-
771 ture and maintaining 6 cm between the blackbody source and the GTS. The results are shown
772 in Figure 14.

773

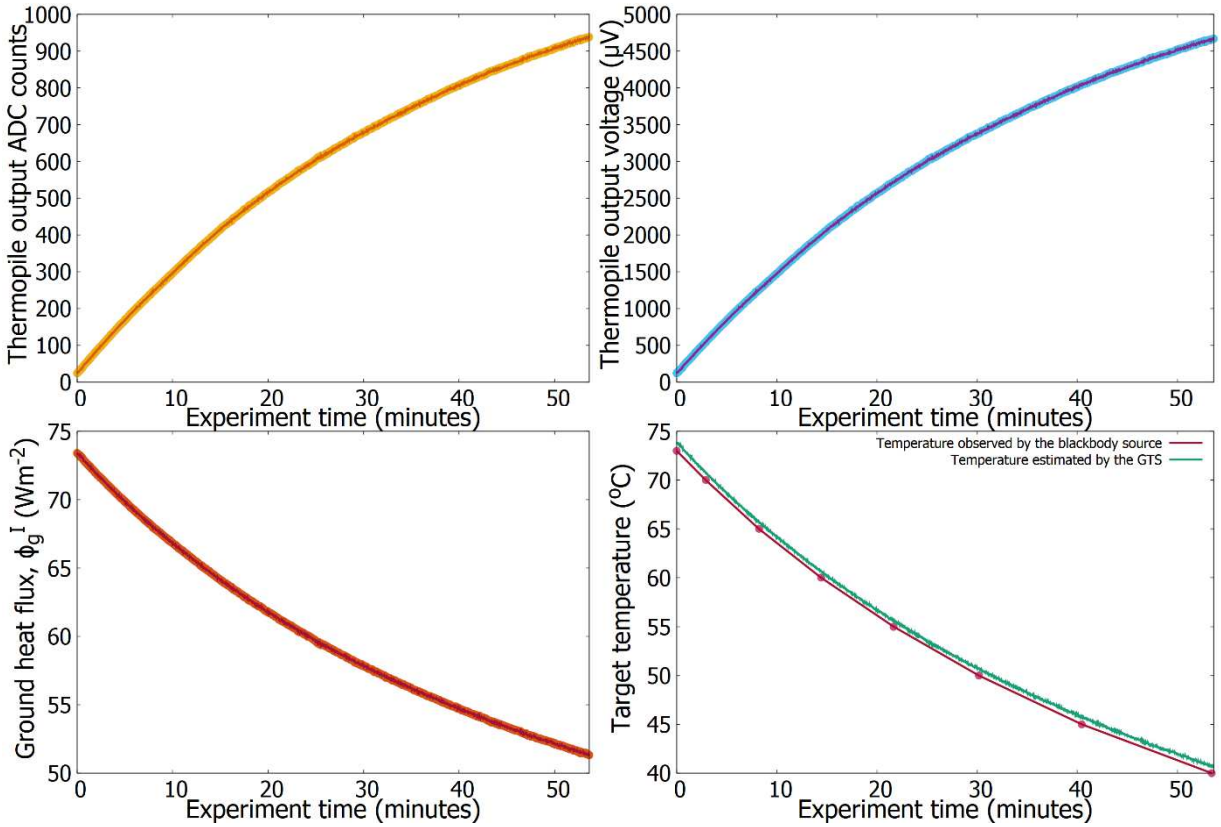

774

775 **Figure 14:** GTS performance tests. The retrieved GTS temperatures obtained using the cali-
776 bration function are shown in d).

We have found that with the current calibration, the error in temperature retrieval is within 0.8 °C. With more calibration data points for intermediate temperatures and more stability, the energy balance model can be improved and thereby the error can be minimized.

5. Ultraviolet Sensor (UVS)

In this section, we present the Ultraviolet Sensor (UVS) design and the calibration tests which have been conducted on the FM, EQM and a UVS engineering calibration prototype. The UVS is located on the top surface of the EU of HABIT, mounted on the Surface Platform deck. It consists of 6 SiC photodiodes designated as UV-A, UV-B, UV-C, UV-D, UV-E and UV-ABC, see Figure 15. Their measurements cover the UV range of 200-400 nm, see Table 1. Table 1 shows the spectral bandwidths of the photodiodes, the nominal gain values of the HABIT electronics and the maximum measurable UV irradiance. The UVS has a solid angle field of view of +/-30° with an unobstructed view of the sky, similarly to the UVS of the REMS sensor on the Curiosity rover (Gomez-Elvira et al., 2012). The UVS of HABIT, along with the REMS-UVS, will enable simultaneous measurements of UV radiation on the martian surface at two different locations on the planet. Each photodiode is housed in a TO-39 package and has an active sensing area of 0.965 mm^2. Each photodiode is placed within a surrounding magnetic ring to deflect airborne, in-falling, magnetic dust particles and mitigate the obstruction of the windows of the sensor by dust. The UVS includes a thermistor to monitor its temperature.

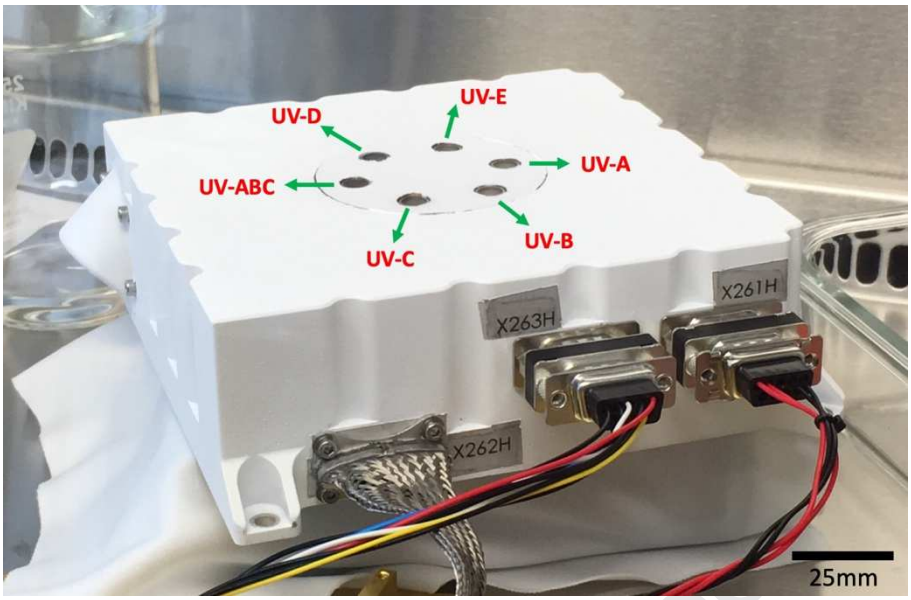

801

802 **Figure 15: UV photodiodes on the top of the HABIT electronic unit. The location of each**

803 **photodiode type is marked with arrows.**

804 **Table 1:** Spectral bands, gain and maximum measurable UV irradiance by the HABIT UVS photodiodes.

805

Channel	Spectral band (nm)	HABIT-UVS Gain (G_i) (mV/nA)	Maximum measurable UV irradiance (W/m^2)
UV-A	335-395	2	28.30
UV-B	280-325	5	8.94
UV-C	220-275	10	3.14
UV-ABC	210-380	0.649	59.46
UV-D	245-290	10	2.93
UV-E	310-335	5	7.38

806

The UV Photodiodes are passive sensors activated by the incident UV radiation that excites the SiC sensor area. Upon excitation, the photodiodes produce a current which is converted, by the HABIT electronics, to voltage values. The maximum allowed output of the UV photodiodes is divided into 4096 ADC levels (12 bits), each one represents a 1mV (with a maximum output of 4.096 V). This gives a sensing resolution limit of 0.024% of the maximum measurable irradiance. The voltage output V_i (mV) obtained from the photodiodes is a function of 4 parameters namely;

(i) Incident spectral radiation $I_i(\lambda)$ (nW/cm^2)

(ii) Sensor spectral responsivity $S(\lambda)$ (A/W)

(iii) Sensor area A_i (cm^2)

(iv) HABIT electronics gain G_i (mV/nA)

Equation (23) shows the integrated spectral radiance over the bandwidth of the UV photodiode, weighted by the spectral responsivity of the sensor and multiplied by the sensing area of the detector. Equation (24) is the voltage that the electronics reads with the gain of the circuit:

$$Current_i = A_i \int_{\lambda_{ai}}^{\lambda_{bi}} S(\lambda)\, I((\lambda) d\lambda \cong R_i^{avg} A_i \int_{\lambda_{ai}}^{\lambda_{bi}} I(\lambda) d\lambda = A_i R_i^{avg}\, I_i^{avg} \quad (23)$$

$$V_i = G_i A_i R_i^{avg}\, I_i^{avg} \quad (24)$$

We can calibrate R_i^{avg} by measuring under a controlled calibrated broadband incident irradiance, the voltage response, knowing the $I_i^{avg} = \int_{\lambda_{ai}}^{\lambda_{bi}} I(\lambda) d\lambda$ incident within the range of response of the sensor

$$R_i^{avg} = \frac{V_i}{A_i G_i I_i^{avg}} \quad (25)$$

or alternatively by calibrating the photodiode spectrally with narrow wavelength excitation beams, as it is done by the manufacturers, and then calculating a weighted average. During operations on Mars, the incident irradiance can be retrieved by converting the output voltage recorded by the UVS electronics, knowing the gain, sensing area and weighted sensor responsivity within the given wavelength range.

$$I_i = \frac{V_i}{A_i G_i R_i^{avg}} \tag{26}$$

The calibration process of UV photodiodes with a monochromator yields their spectral responsivity $S(\lambda)$ at normal incidence and ambient temperatures. Other tests are focused on estimating the linearity and the dependence on the angle of incidence of the direct solar beam. The angular tests have been performed with the FM and EQM HABIT EU at ambient conditions, whereas the temperature dependence tests are performed in a thermally controllable chamber. The calibration procedures are described next.

Spectral calibration:

The spectral responsivity of the UV photodiodes is obtained by measuring the response of each photodiode to a narrow wavelength excitation beam of ~5nm, at normal incidence and ambient temperature. The UVS spectral calibration setup is shown in Figure 16. It consists of a Deuterium UV lamp (Avantes), focusing optics, UV-VIS monochromator (Newport), filter wheel (Newport) with 3 ND filters, fiber optic cables with beam splitter, a power meter (Newport) along with 818-UV/DB photodetector to measure the strength of UV radiation and a UV/VIS/NIR spectrometer (Avantes). Figure 17 shows the relative spectral responsivity of

the UV-A, UV-B, UV-C, UV-D and UV-ABC photodiodes from the spectral calibration tests, the UV-E curve is shown from the data provided by the manufacturer.

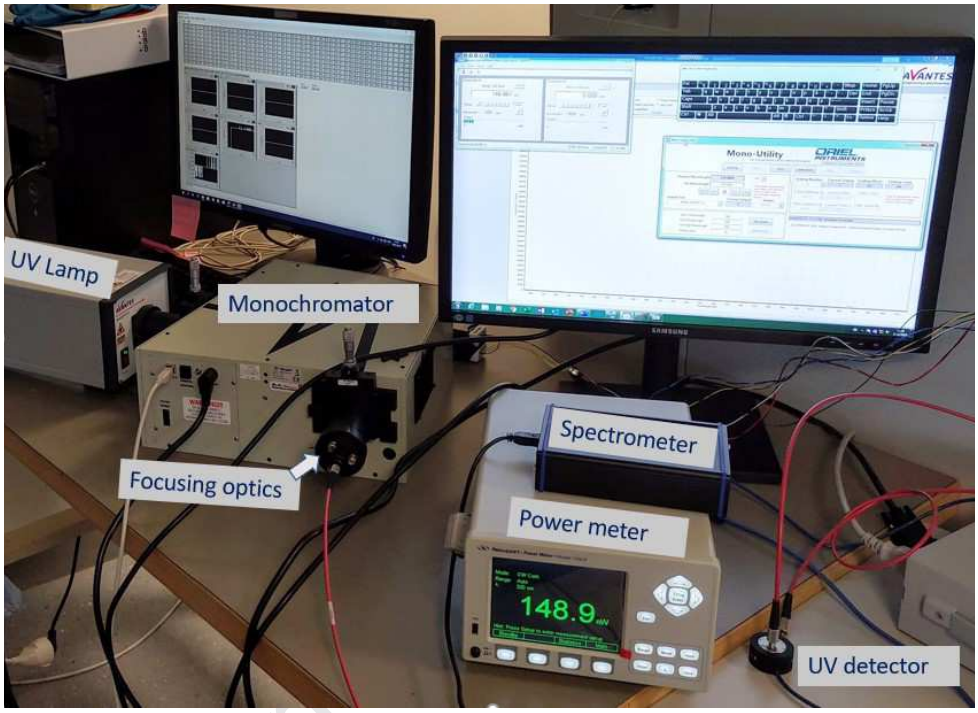

Figure 16: UVS calibration workbench consisting of the required instruments for the calibration of UV photodiodes.

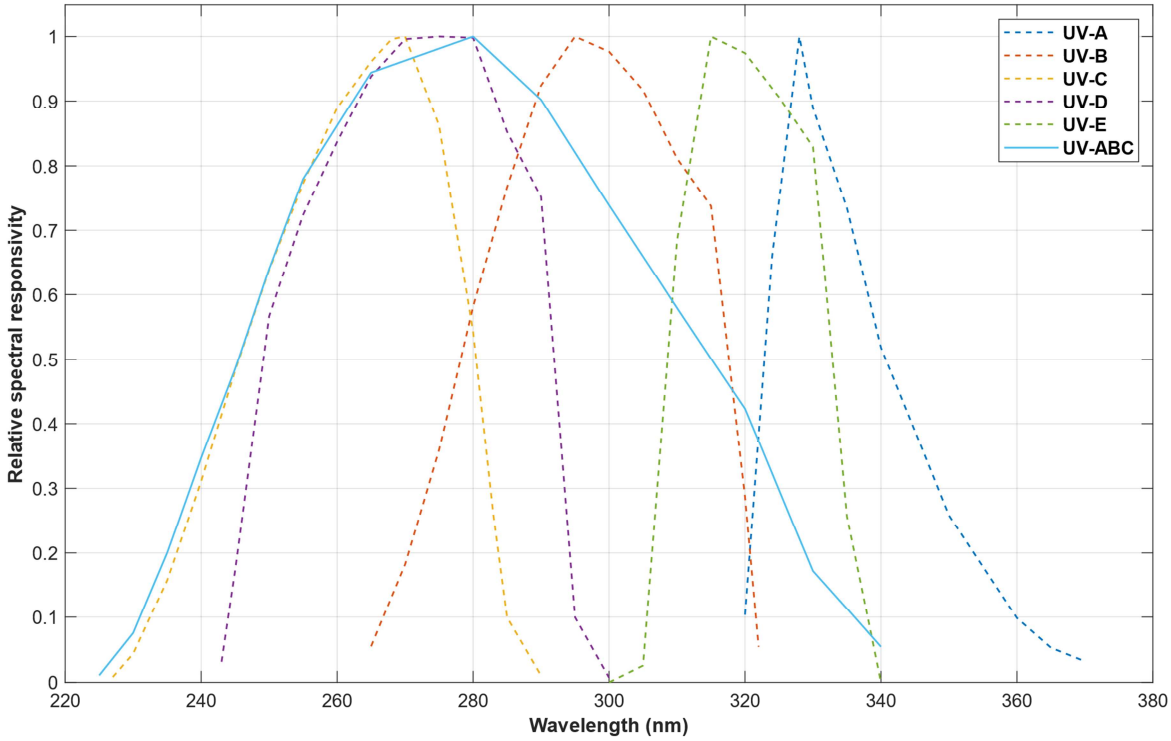

Figure 17: Relative spectral responsivity of the HABIT UV photodiodes.

Linearity test:

The linearity tests have been performed with the FM at ambient conditions in a cleanroom. The neutral density (ND) filters on the filter wheel housing with optical densities (OD) 0.04, 0.1 and 0.5 are used while maintaining all other parameters constant, namely the focusing, bandwidth, and wavelength. Figure 18 shows the normalised linearity of the photodiodes UV-A, UV-B, UV-C, UV-D and UV-E. The photodiodes UV-A, UV-B and UV-E show better than 2.5% linearity for the described test conditions, while UVC and UVD show linearity better than 11.38% and 3.06% respectively. The large errors in linearity shown by the UV-C and UV-D channels compared to the rest are induced due to their sensitivity to the ozone absorp-

tions in the air column under Earth laboratory conditions. The linearity calculation errors for these two photodiodes can be improved in future tests under neutral atmosphere conditions.

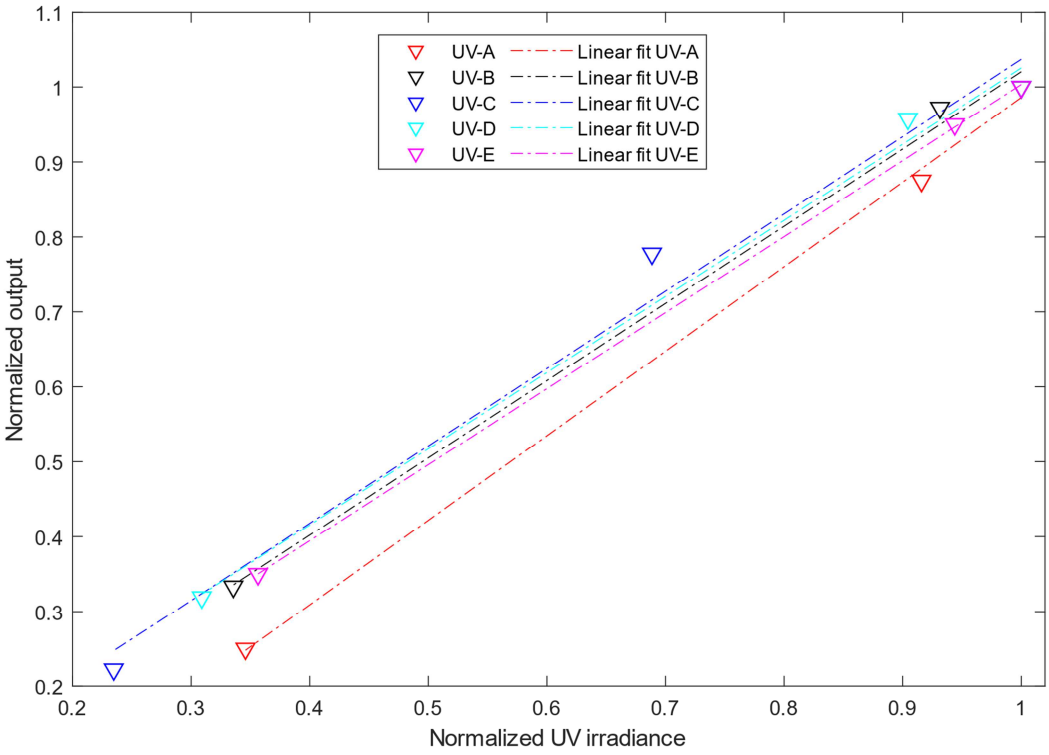

Figure 18: Normalized linearity graph of UVS photodiodes. The X-axis shows the normalised UV irradiance power and Y-axis shows the normalised output of the photodiodes and the dotted lines represent the linear fit curves for the response of the photodiodes.

R-test:

The R-tests are conducted to derive the average responsivity, R_i^{avg} of the UVS photodiodes a constant value which is wavelength-independent and can be used to obtain in real-time a quick estimate of the incident irradiance without prior knowledge of the spectral shape of the incident irradiance. Among the six UVS photodiodes, the UV-A channel has minimum sensitivity to ozone absorption and atmospheric effects from the air column. Next, we describe for

illustration the procedure of the R test for the UVA and UVB photodiodes with an engineering calibration prototype. The sensing area is illuminated with the full-strength signal from the Deuterium UV lamp using the fibre optic cable and COL-UV/VIS collimating lens at 10 mm distance from the photodiode. The output current from the photodiode is recorded using HM8112-3 precision multi-meter and the power of the incident UV radiation is recorded using the power meter 1936-R connected with the 818-UV/DB low power UV enhanced silicon photodetector. The incident UV power is measured at the wavelengths of the UVA or UVB spectral band and the mean power is substituted for I_i^{avg} in Equation (1) to calculate the average spectral responsivity, resulting in $R_A^{avg} = 0.0596 \frac{A}{W}$ and $R_B^{avg} = 0.2438 \frac{A}{W}$. At the time of submission of this work, the averaged spectral responsivity for the other photodiodes is still pending calibration. We include for reference an estimate of the order of range of R using the Full Width at Half Maximum (FWHM) of the spectral response as provided by the manufacturer, see Table 2. These values shall be updated with future calibrations of the EQM when the model returns from IKI after the tests of the ExoMars program. The REMS UV channel-averaged responses are included for comparison.

Table 2: Reference R^{avg} values of the HABIT-UVS photodiodes.

Channel	R_i^{avg} (A/W) HABIT 25°C	R_i^{avg} (A/W) REMS 25°C
UV-A	0.0596	0.0529
UV-B	0.2428	0.1946
UV-C	0.111 (FWHM)	0.0716
UV-D	0.1293 (FWHM)	0.0602
UV-E	0.103 (FWHM)	0.0907
UV-ABC	0.1276 (FWHM)	0.1008

Temperature dependence test:

The spectral response of the SiC UV photodiodes increases with temperature, approximately 1% per degree, due to small variations of the quantum efficiency of SiC detectors and possibly also due to changes in the spectral response of the filters. This makes the output shift towards longer wavelengths beyond 280 nm. Thus, photodiodes UV-A, UV-E and partly UV-B whose spectral response is higher than 280 nm are more sensitive to the temperature changes (Gomez-Elvira et al., 2012). The responsivity of the electronics can also vary with temperature. The UVS is within the Electronic Unit (EU), on the Surface Platform deck, and it is protected with a heater that is activated when its temperature is below -33℃ and disabled if the temperature of the surface platform rises above -30℃, we, therefore, limit the tests to the range -40°C to 25 °C (ambient conditions to compare with the rest of calibrations).

Figure 19 shows the temperature dependence test workbench along with the engineering prototype inside the thermal chamber with the photodiodes and the collimating lens in normal incidence orientation. This test uses an HM8112-3 precision multi-meter from Rohde and Schwarz that measures the current across the UV photodiodes, a deuterium UV lamp from Avantes and a temperature measurement unit made using Arduino, MAX31865 and PT1000 RTD. The UVS engineering calibration prototype houses the same UV photodiodes used in the HABIT flight model. A Heraeus Votsch HT4010 climate chamber is used. A single-mode fibre optic cable of core diameter 800 μm was used to couple the deuterium UV lamp and the collimating lens thereby utilising the full spectrum UV radiation from the UV lamp. The distance between the collimating lens and the UV photodiodes is kept constant at 10 mm during the tests. Sufficient warm-up time is provided for the UV lamp to obtain a stable output before proceeding with the tests. The temperature measurements are obtained from the PT1000

RTD sensor mounted close to the UV-photodiodes as shown in Figure 19. The data from the multi-meter and the PT1000 temperature sensor is logged at a frequency of 1 Hz. Figure 20 shows, an illustration, the relative change of the response with respect to the nominal ambient response for UV-ABC and UV-C. Once on Mars, for a given temperature of the photodiodes, the temperature correction factor can be interpolated from these data.

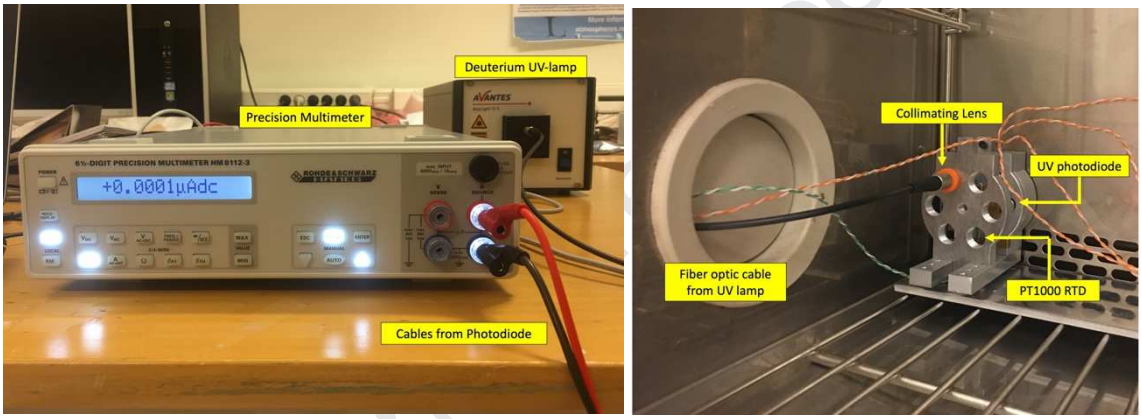

Figure 19: (left) Temperature dependence workbench (right) UVS engineering proto-type inside the climate chamber.

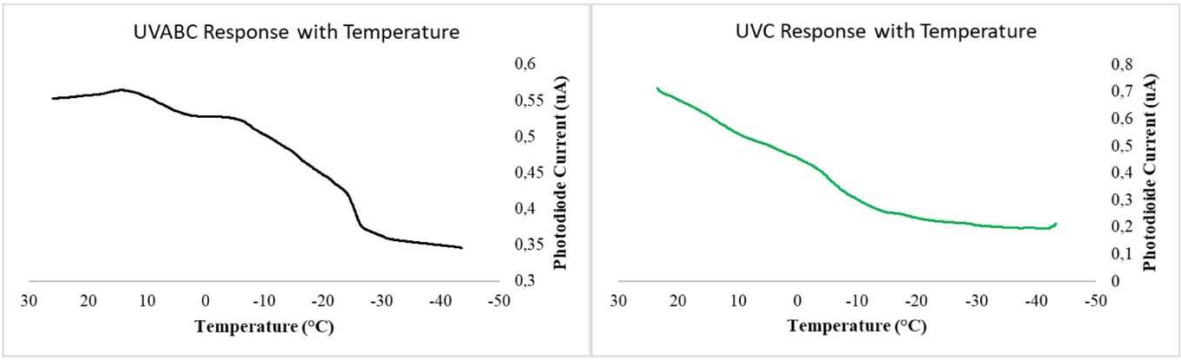

Figure 20: Variation of the UV photodiode current response with temperature.

Incidence angle dependence test:

The direct beam of UV radiation from the Sun reaches the photodiode with an angle of incidence that varies as the Sun moves in the sky. It depends on the hour of the day and the season, and of course on the landing site and surface platform inclination. This information can be obtained as ancillary data during the operation on Mars. The REMS UVS photodiodes follow a $cos^{a}(\theta)$ response, as long as the direct beam is within the nominal field of view of +/- 30° (Zorzano et al., 2009; Gómez-Elvira et al., 2012). This exponent is next calibrated for HABIT. To modify precisely the angle of incidence, a dedicated fixture was designed, see Figure 21. It consists of a twin linear actuator, a screw-driven mechanism and a micro-stepper motor with an open-loop control in the x-y axis.

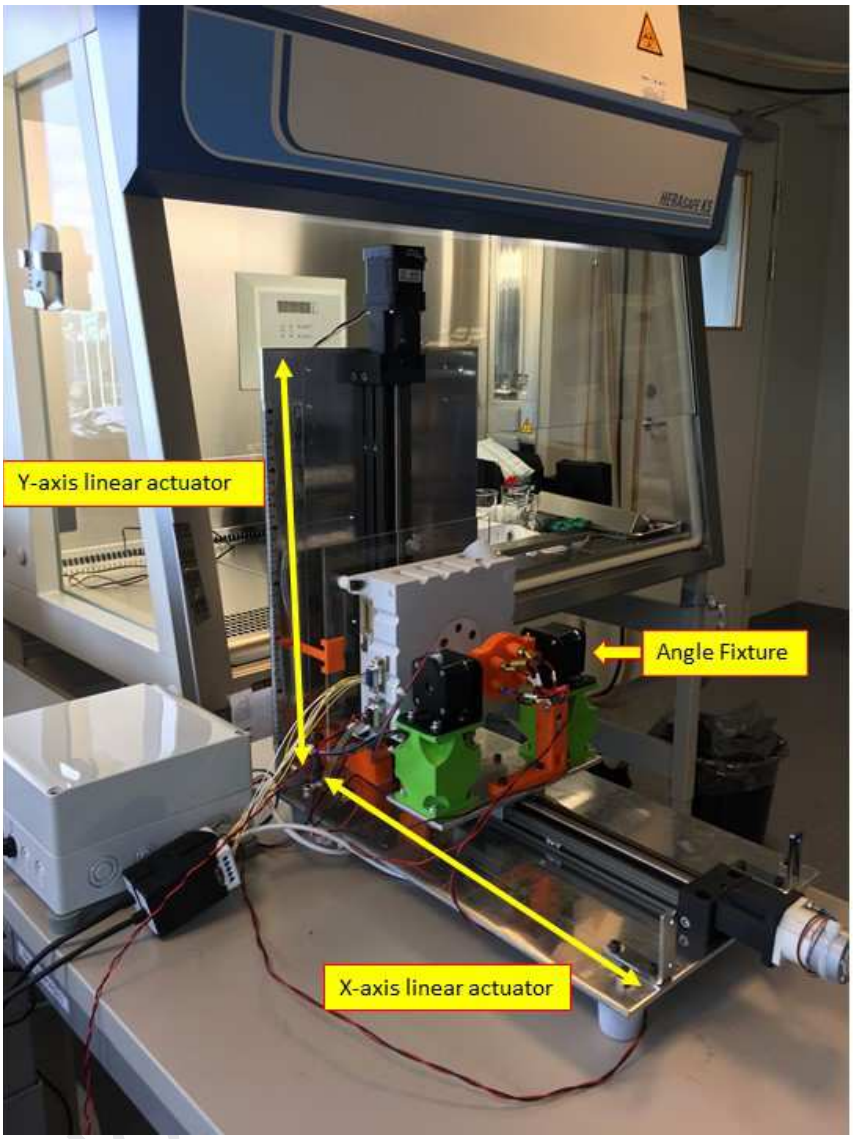

963

964 **Figure 21: Mechanical fixture for incidence angle dependence tests on which the EU of**

965 **HABIT EQM is fixed.**

966 The angle of incidence test was performed at ambient conditions for 0 to 30° incidence angle,

967 at increments of 5°. A 340 nm 0.33 mW UV LED 341 nm from Thor labs was utilised as the

968 UV source during the incidence angle test. The distance between the UV photodiode and the

969 UV LED was accurately maintained at 6 cm. Figure 22 shows an example of the calibration

970 curve, and the fit to $a\,cos^n(\theta) + b$ for the UVA photodiode. The parameters of the fit for the

971 UVA sensor are: n_{UVA}=15, a_{UVA}=24, b_{UVA} =29.

972

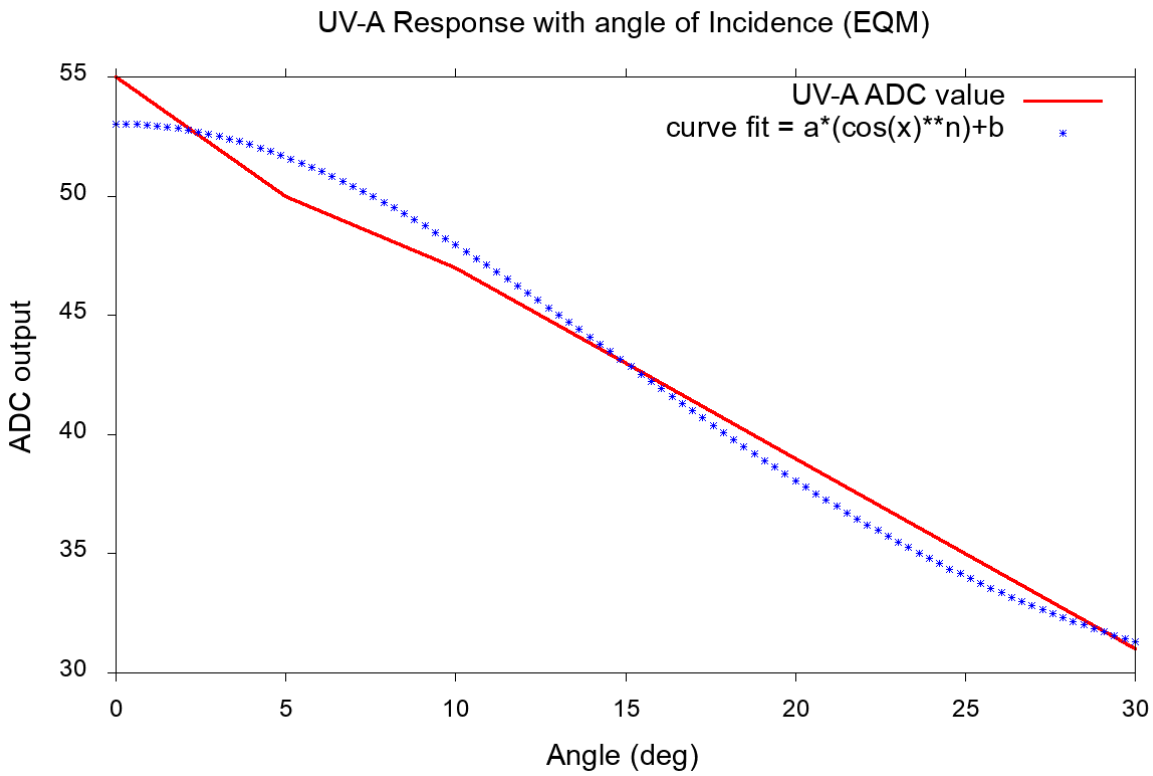

Figure 22: UV-A photodiode cosine angle dependence response.

6. Brine Observation Transition To Liquid Experiment (BOTTLE)

6.1 Design and operation of BOTTLE

The Brine Observation Transition To Liquid Experiment (BOTTLE) shall monitor the formation and stability of liquid brines on Mars. It consists of 6 cells, shown in Figure 23. Four of them are exposed to the Mars environment and contain deliquescent salts that have been found on Mars (calcium-chloride $CaCl_2$, ferric-sulphate $Fe_2(SO_4)_3$, magnesium-perchlorate

$Mg(ClO_4)_2$, and sodium-perchlorate $NaClO_4$). The other 2 cells are empty will be used to monitor the air electrical conductivity and collect atmospheric dust.

The salts are exposed to the martian environment through a High Efficiency Particulate Air (HEPA) filter (to comply with planetary protection protocols). The deliquescence process of salts will be monitored by observing the changes in the electrical conductivity (EC) of each cell with the electrode pairs at three different levels (denoted as low, mid and high). Gold electrodes are used for better resistance to corrosion (Nazarious et al., 2019). This technique has been commonly used for the detection of liquid or frozen water in soils (McKay et al., 2003; Davis et al., 2010). Previous studies have suggested electrical conductivity as a good method to monitor the deliquescence process of salts (Yang et al., 2006; Heinz et al., 2016). The electrical conductivity measurements correlated well with the deliquescence rates of mixtures of martian analogue soil and perchlorates or chlorides. The electrical conductivity method provides a time series and may be a good indicator of the brine formation process, with higher sensitivity than either Raman spectroscopy or estimates based on deliquescence relative humidity (Heinz et al., 2016). The salts of BOTTLE have the property of absorbing water from the martian atmosphere, forming different hydrates, and brines, depending on the temperature and relative humidity; and we expect to identify the phase changes from dry salt to its hydrate forms, to liquid brine or to frozen brine.

BOTTLE is equipped with a PT1000 temperature sensor to serve as reference and a 12 W heater (at Pulse Width Modulation with 100% duty cycle) to allow recyclability of salts. The purpose of the heater will be to: 1) dehydrate the liquid brine to anhydrous salt and restart the experiment, and 2) provide inflight calibration for detecting any degradation in the hardware and correct the offsets. The experiments on BOTTLE will show the absorption and release of

water and will serve to demonstrate the ISRU potential of the instrument to collect water for the future exploration of Mars.

6.2 Measurements and calibration of BOTTLE EQM and FM

BOTTLE measures the current flow, *I* and the voltage drop, *V* across low, mid and high electrode pairs (see figure 23) of each of the six cells, along with the CU temperature. Consequently, the conductance, *G* in Siemens is calculated with equation (27).

$$G = \frac{I}{V}\ (S) \qquad (27)$$

BOTTLE uses a 2.048V bias voltage and have two mode of conductance measurements. The high conductance mode uses a 70 mV electric pulse and a 100 Ω current sense resistor while the low conductance mode uses a 700 mV electric pulse to generate enough current for measurements and a 10 kΩ resistor. At the beginning of every data acquisition session, BOTTLE measures in high conductance mode by default. The mode is switched to low, when the measurement is out of range. The first 8 samples are used as a filter to make a smooth transition between the modes and thus these 8 measurements must be discarded for interpretation.

Laboratory experiments for evaluating the coefficients of the calibration function were performed for 100 data points at a frequency of 1000 ms. The measured conductance of the sample is translated to electrical conductivity by multiplying with the geometrical cell constant of the electrode pair, K_{cell} as in equation (28).

$$\sigma_{measured} = K_{cell} \times G\ (\mu S cm^{-1}) \qquad (28)$$

The geometrical cell constant of the electrode pair depends on its physical dimensions. There are three electrode pairs each in four middle cells and two electrode pairs each in the two end cells summing to a total of 16 electrode pairs and consequently 16 geometrical cell constants are to be calculated with equation (29).

$$K_{cell} = \frac{Distance\ between\ electrodes\ (in\ cm)}{Surface\ area\ of\ electrodes\ (in\ cm^2)} = \frac{d}{A} \qquad (29)$$

where, A_{low} = 1.6 cm × 0.4 cm = 0.64 cm^2

A_{mid} = 1.6 cm × 0.2 cm = 0.32 cm^2

A_{high} = 1.6 cm × 0.2 cm = 0.32 cm^2

The distance between the electrode pairs are measured using an optical measurement system (Mitutoyo MF 176) to verify the alignment of the electrodes and to obtain an accurate geometrical cell constant of the electrode pairs. The minimum and maximum distances between each of the electrode pairs are averaged. A screenshot of the procedure used to measure the distances in the CAD model constructed with the optical measurements is shown in Fig. 23 and the computed cell constants are provided in Table 3.

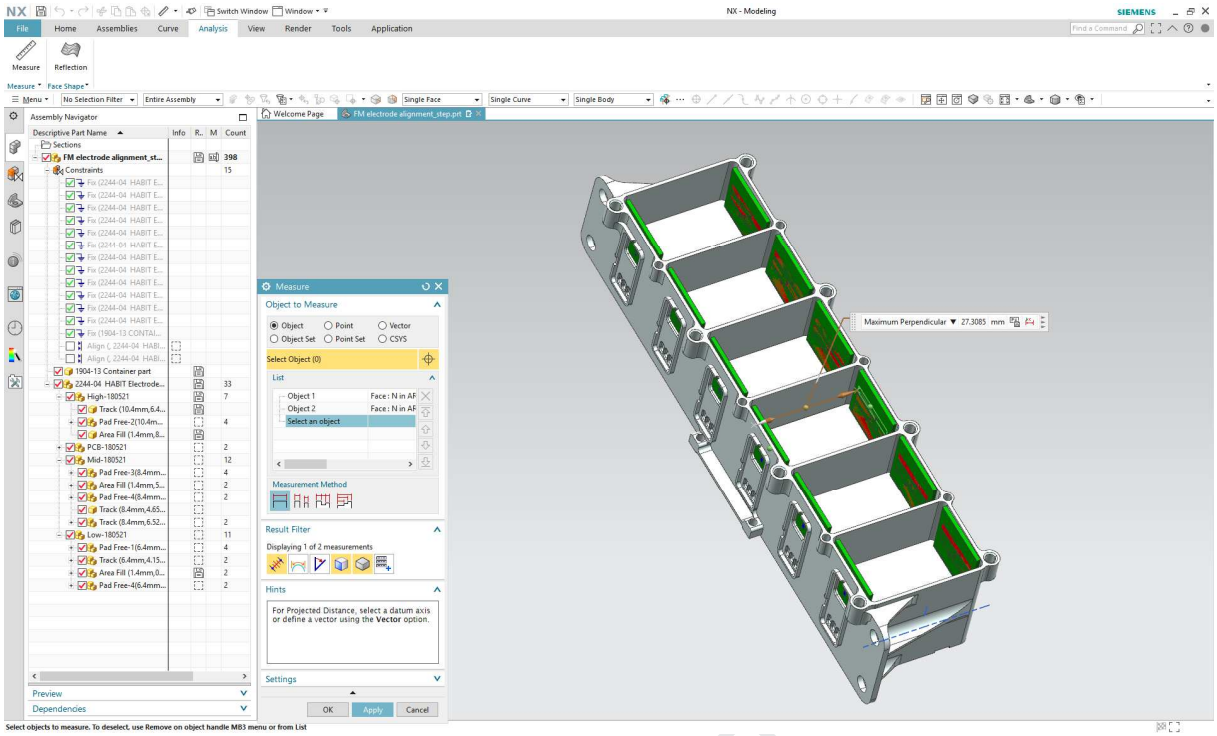

Figure 23: CAD model of BOTTLE flight model generated using the measurements from the optical measurement system.

Table 3: Computed geometrical cell constants of all the electrode pairs.

Electrode designation	d (cm)	A (cm^2)	K_{cell} (cm^{-1})
Cell-1, Low	2.7124	0.64	4.2381
Cell-1, Mid	2.6985	0.32	8.433
Cell-2, Low	2.7361	0.64	4.2752
Cell-2, Mid	2.7335	0.32	8.5421
Cell-2, High	2.7313	0.32	8.5354
Cell-3, Low	2.7412	0.64	4.2832
Cell-3, Mid	2.7352	0.32	8.5476
Cell-3, High	2.7312	0.32	8.5351
Cell-4, Low	2.7363	0.64	4.2755
Cell-4, Mid	2.7322	0.32	8.5382
Cell-4, High	2.7289	0.32	8.5279

Cell-5, Low	2.7402	0.64	4.2816
Cell-5, Mid	2.7312	0.32	8.5349
Cell-5, High	2.7246	0.32	8.5144
Cell-6, Low	2.7294	0.64	4.2646
Cell-6, Mid	2.7226	0.32	8.5082

6.2.1 Zero offset or dry point

The purpose of this experiment is to obtain the zero or dry point for determining the calibration function coefficients. This test was performed with the BOTTLE flight model, inside a vacuum chamber at a temperature between 26.27 °C and 26.32 °C and measuring the empty cells with only the natural noise frequency of the instrument electronics. The measured electrical conductivity in the vacuum conditions is used as a reference for the absolute zero measurement 0.00364 μScm^{-1}, averaged across all the low electrodes.

6.2.2 Calibration function and coefficients

The calibration function was determined with several calibration standards with known electrical conductivity values. During this calibration procedure, we used the conductivity standards: 84 μScm^{-1}, 1413 μScm^{-1}, 5000 μScm^{-1}, 12880 μScm^{-1}, 80000 μScm^{-1} and 111800 μScm^{-1} as shown in Figures 24 and 25. As we will show later in the experiments of the SpaceQ, our EC range of interest is from 0 to 1000 μScm^{-1}, as the maximum EC we have observed with a deliquescent forming brine under martian conditions is of the order of 100 μScm^{-1}. We increase the region of interest by one order of magnitude.

Figure 24: Procedure to fill the calibration standards in BOTTLE cells in a clean laminar fume cabinet at ambient temperature.

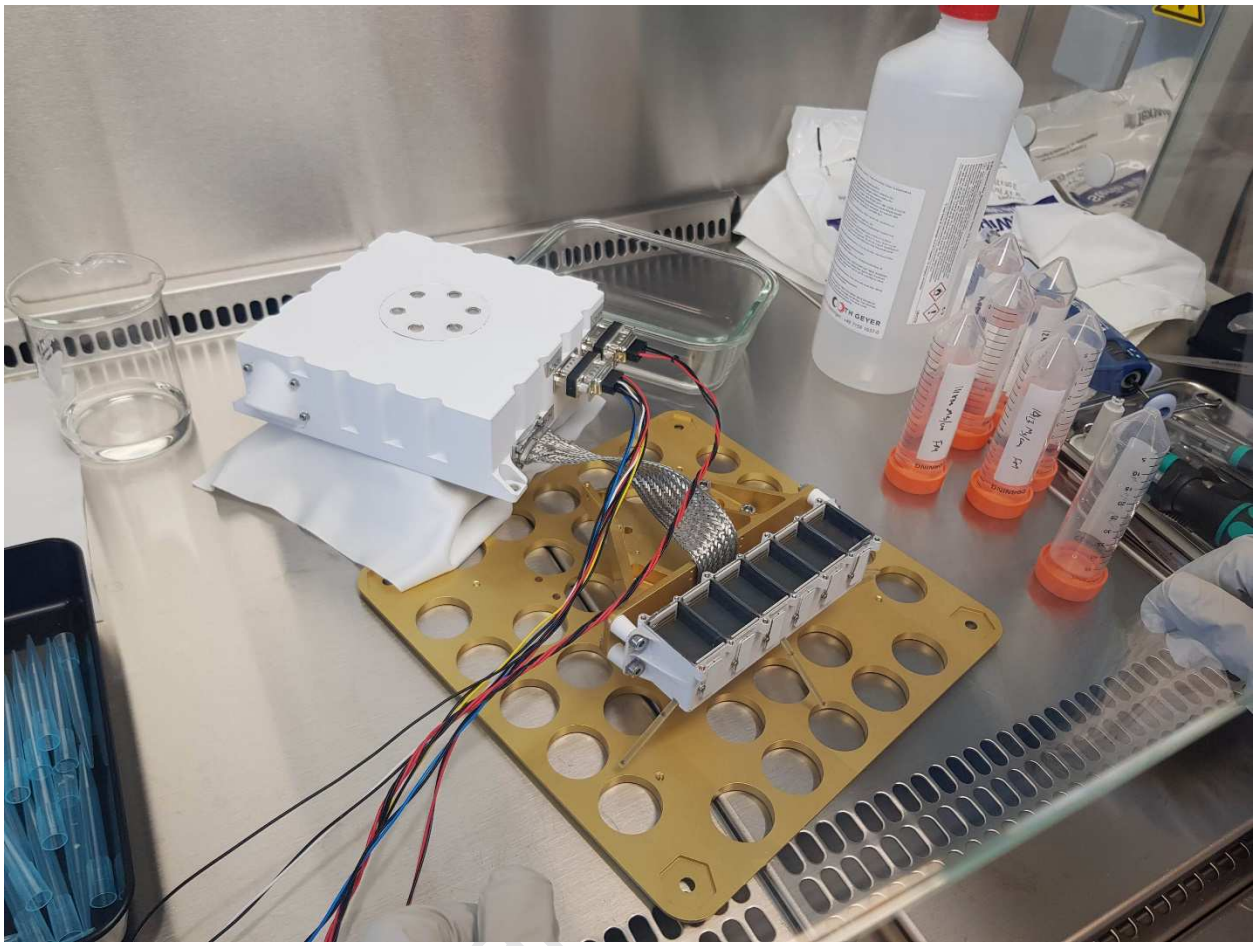

Figure 25: A view of the BOTTLE flight model in the laminar fume cabinet with calibration standards filled in the cells.

The calibration function was determined from these calibration standard measurements with a least square regression, by fitting a 2nd order polynomial curve as in equation (30). For a better interpretation of the BOTTLE measurements, the specific choice of the two calibration standards will be chosen depending on the required accuracy within a certain measurement range (two-point calibration).

$$\sigma_{actual} = a_2 \sigma^2_{measured} + a_1 \sigma_{measured} + a_0 \, (\mu S cm^{-1}) \quad (30)$$

We obtain 16 calibration function coefficients, where each corresponds to an electrode pair. The advantage of having multiple calibration points is to use them depending on the desired measurement range and to fine-tune the resolution of measurements within a specified range. By default, we use the calibration function derived with zero point, 84 μScm^{-1} and 1413 μScm^{-1} (two-point calibration). But, if the measured EC is over 1413 μScm^{-1}, additional calibration points (5000 μScm^{-1}) can be included to extend the measurement range of the instrument. Also, in order to measure the 2000 μScm^{-1} accurately, a new set of calibration function coefficients can be computed only using the 1413 μScm^{-1} and 5000 μScm^{-1} points. Figure 26 shows the full extent of the calibration points with the 0 to 1413 μScm^{-1} plot shown in the inset.

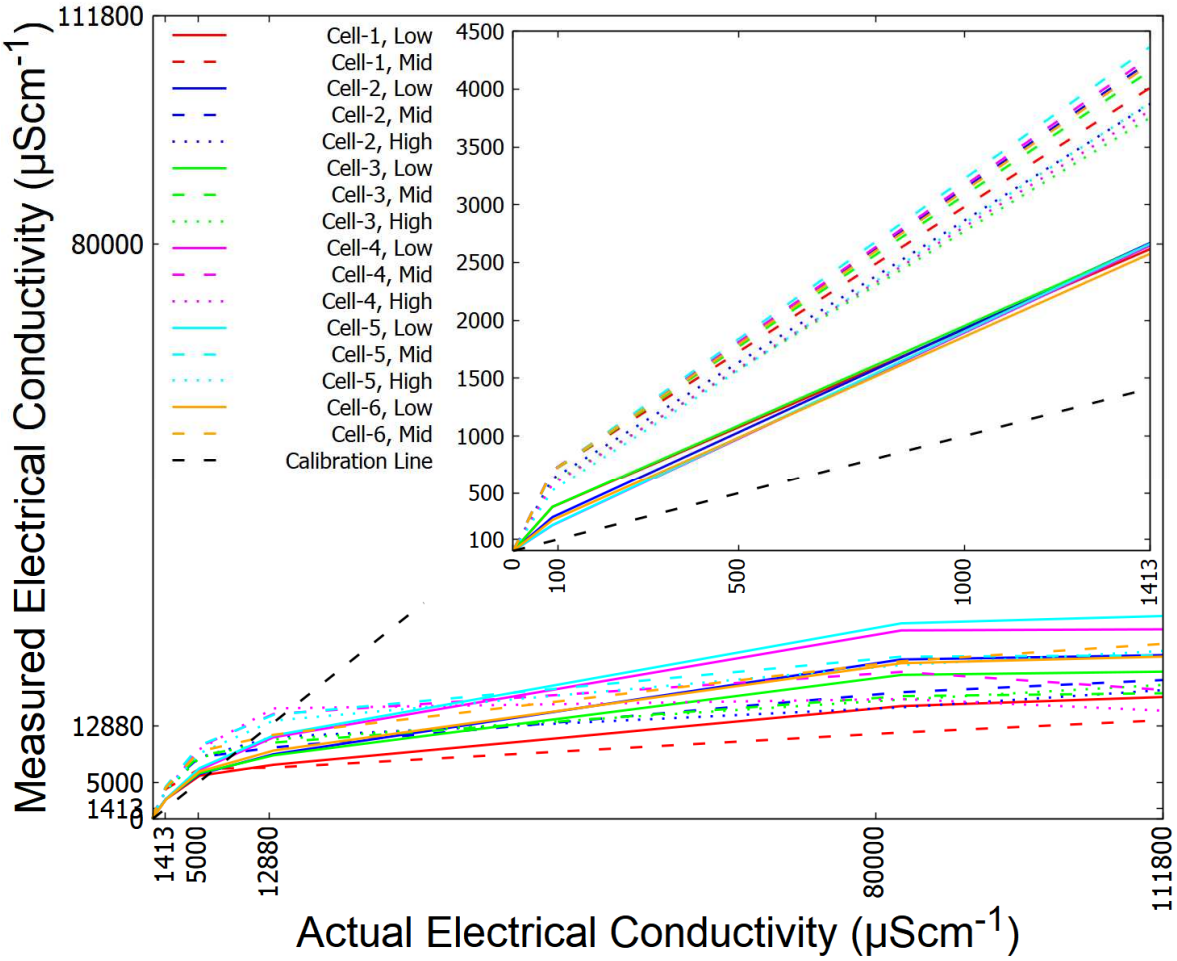

Figure 26: A comparison of the measured electrical conductivity by BOTTLE flight model with the actual electrical conductivity of the calibration standards, where the standard solutions were covering until the high electrode. Similarly, EC measurements were carried out for low and mid electrode coverages (not shown in this figure). Lower conductivities show better accuracy with the calibration standards while the higher conductivities deviate from the calibration line (black). (inset) A comparison of the measured electrical conductivity by BOTTLE flight model with the actual electrical conductivity of the calibration standards in the lower electrical conductivity range between 0 and 1413 µScm^{-1}.

We compute the calibration function coefficients by covering the three levels of electrode for each conductivity standard. Therefore, we have three sets each of 16 calibration function coefficients (total of 48) for low, mid and high electrode coverage. While converting the raw

measured electrical conductivity to the actual values, one of these set of coefficients will be utilized depending on the coverage of salts in the low, mid or high electrode. In its initial configuration during FM delivery, the salts covered until low electrode and thus the 16 calibration function coefficients corresponding to low electrode overage will be initially used. As the experiment progresses and the brine level increases, the use of a different set of coefficients (mid or high) may be recommended. The information about the coefficients used will be flagged in the HABIT PSA data bundle. Table 4 shows the 48 calibration function coefficients.

Table 4: Calibration function coefficients for each electrode pair with low, mid and high electrode coverages.

Electrode designation	Electrode coverage								
	Low			Mid			High		
	a_2	a_1	a_0	a_2	a_1	a_0	a_2	a_1	a_0
Cell-1, Low	0.000287	0.333303	-0.01185	0.000170	0.216503	-0.00770	0.000134	0.178402	-0.00634
Cell-2, Low	0.000272	0.299276	-0.00790	0.000127	0.289159	-0.00764	9.315e-05	0.271738	-0.00718
Cell-3, Low	0.000283	0.329932	-0.01238	0.000161	0.218174	-0.00819	0.000128	0.179918	-0.00675
Cell-4, Low	0.000308	0.285631	-0.00642	0.000162	0.214088	-0.00481	5.559e-05	0.380646	-0.00855
Cell-5, Low	0.000283	0.295427	-0.01459	0.000161	0.214926	-0.01061	5.529e-05	0.377817	-0.01866
Cell-6, Low	0.000294	0.312369	-0.01462	0.000172	0.207752	-0.00973	9.218e-05	0.302299	-0.01415
Cell-1, Mid	0	0	0	8.917e-05	0.111435	-0.00285	6.612e-05	0.078964	-0.00202
Cell-2, Mid	0	0	0	7.842e-05	0.118968	-0.00778	5.692e-05	0.084491	-0.00552
Cell-3, Mid	0	0	0	8.426e-05	0.115198	-0.00244	5.966e-05	0.084016	-0.00178
Cell-4, Mid	0	0	0	7.381e-05	0.123625	-0.01022	5.539e-05	0.086063	-0.00712

Cell-5, Mid	0	0	0	7.175e-05	0.116869	-0.00487	5.207e-05	0.089149	-0.00371
Cell-6, Mid	0	0	0	7.782e-05	0.117713	-0.00508	5.758e-05	0.084977	-0.00367
Cell-2, High	0	0	0	0	0	0	6.716e-05	0.09683	-0.00480
Cell-3, High	0	0	0	0	0	0	7.004e-05	0.105298	-0.00788
Cell-4, High	0	0	0	0	0	0	6.535e-05	0.113147	-0.00632
Cell-5, High	0	0	0	0	0	0	5.676e-05	0.136389	-0.01211

6.3 Validation

This experiment is designed to validate the evaluated calibration function. Using zero, 84 μScm^{-1} and 1413 μScm^{-1} calibration points to determine the calibration function coefficients, we applied it back to the measurements with the 1413 μScm^{-1} calibration standard solution. Figures 27 to 29 shows the calibrated electrical conductivity values of 1413 μScm^{-1} after applying the calibration function. For this experiment the mean EC error with respect to the standard was computed to be +70/-90 μScm^{-1} (averaged between low, mid and high electrode measurements).

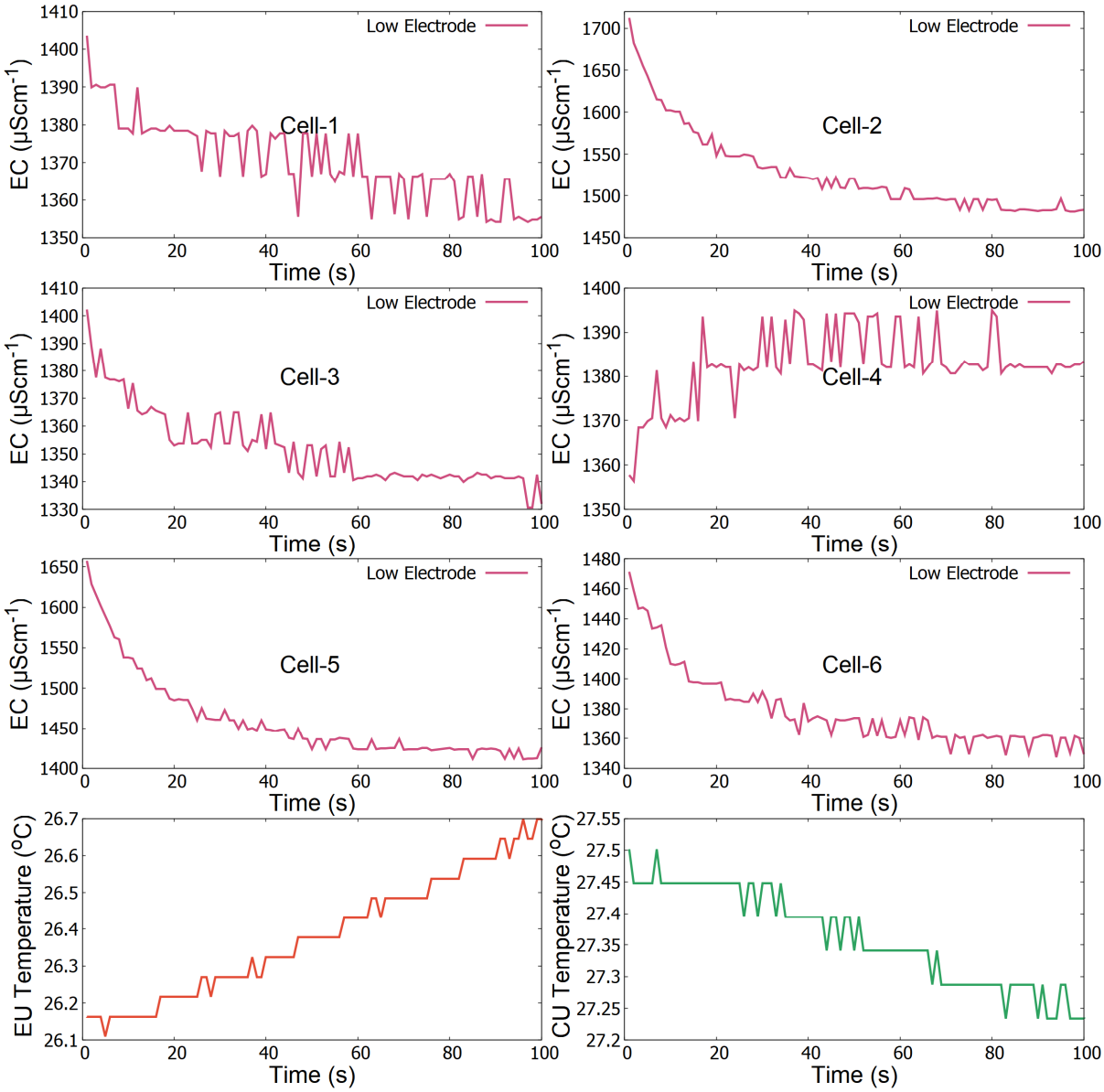

1144

1145 **Figure 27:** Measurements of the 1413 µScm^{-1} calibration standard covering the low electrode.
1146 The actual electrical conductivity was computed using the calibration function coefficients
1147 corresponding to the low electrode coverage. Only the low electrode EC measurements are
1148 shown for clarity.

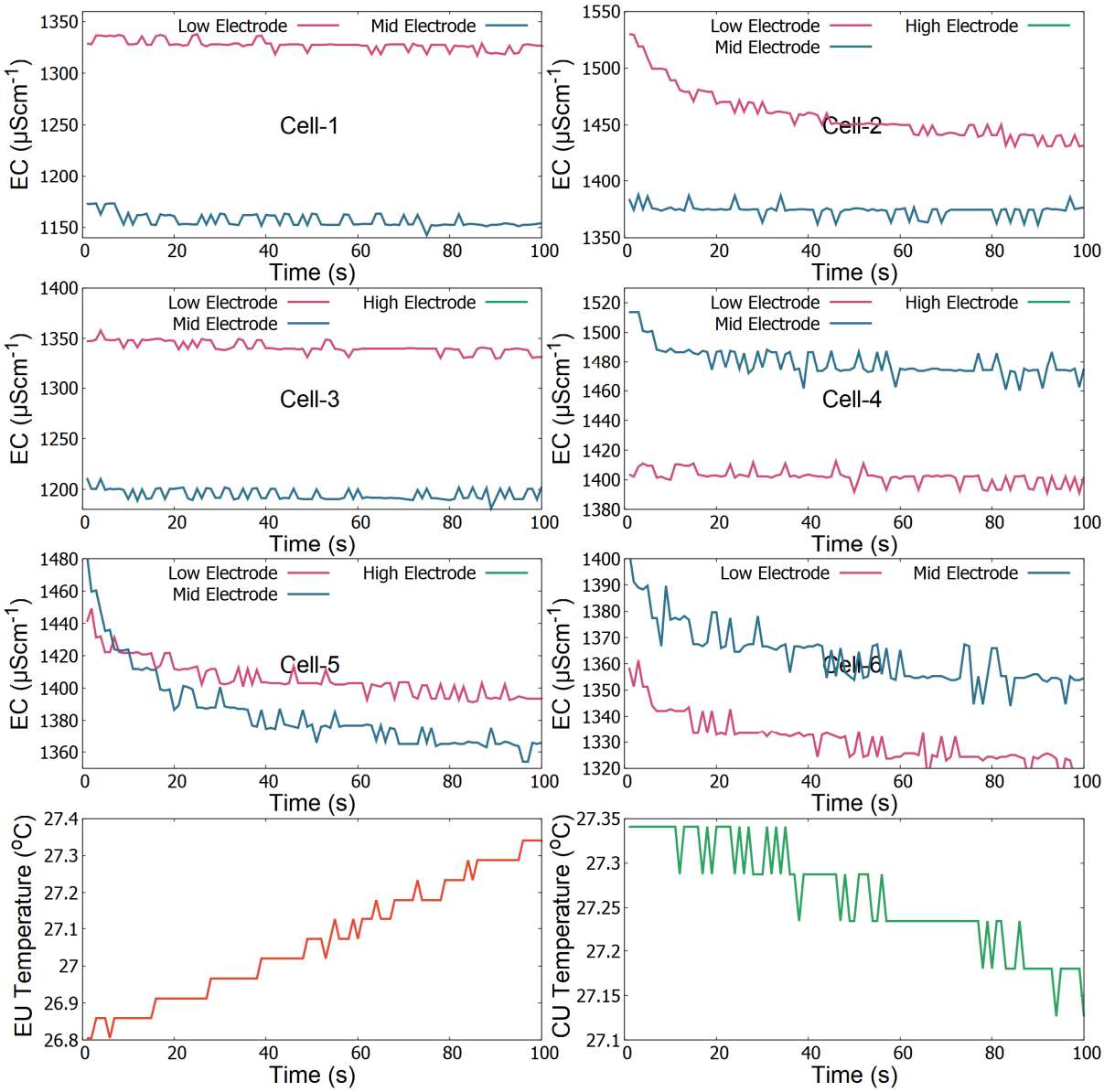

1149

1150 **Figure 28:** Measurements of the 1413 µScm^{-1} calibration standard covering the mid electrode.

1151 The actual electrical conductivity was computed using the calibration function coefficients

1152 corresponding to the mid electrode coverage. Only the low and mid electrode EC measure-

1153 ments are shown for clarity.

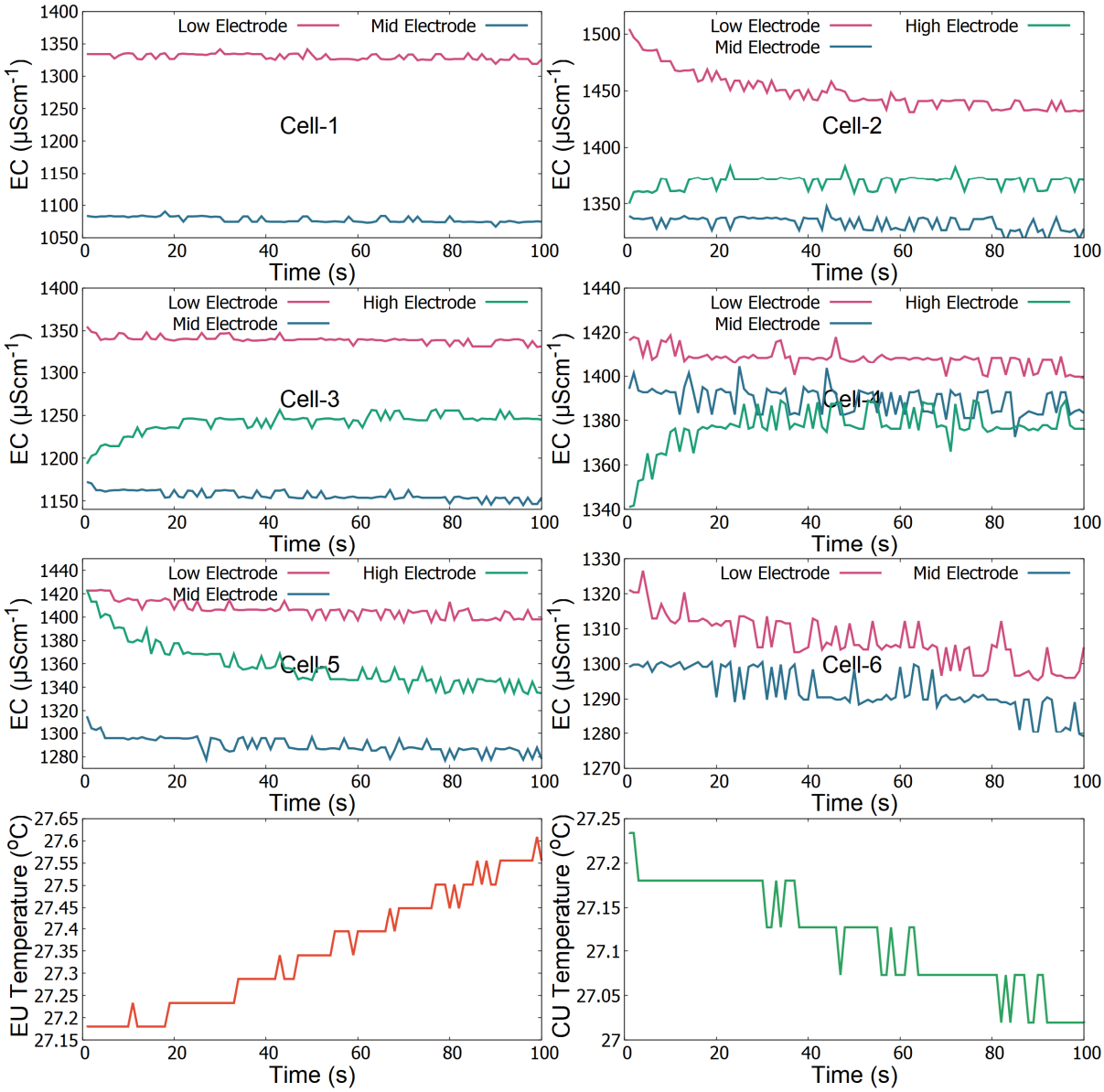

Figure 29: Measurements of the 1413 µScm^{-1} calibration standard covering the high electrode. The actual electrical conductivity was computed using the calibration function coefficients corresponding to the high electrode coverage. EC measurements are shown for all electrodes.

6.5 Clean-room measurement of dry salts in FM

Figure 30 shows an example of BOTTLE measurements performed with the FM in the clean-room of Thales Alenia Space-France (TAS-F) during integration in the Surface Platform. The EC values are of the order of ~0.1 µScm^{-1}, for all the containers, including the ones that only

have sealed ambient air. This demonstrates the proper sealing of the containers, and the dry state of the salts. When the EC of the salts is equal (or lower) than that of the pure air, that shows that no hydration has taken place, and the dominant component of the EC is the one of the air voids between the salt grains. On the other hand, the EC of the air depends on the amount of water, which in turn depends on the pressure (Earth or martian) and the relative humidity. The reported value of 0.1 μScm^{-1} is the one we expect under Earth environmental conditions. However, as mentioned above this value is as low as 0.00364 μScm^{-1} for vacuum tests in the thermal vacuum facility. And as we shall show later on, this value goes to values as low as 10^{-8} μScm^{-1} when the experiments are run at martian pressures, and any remaining water molecule is flushed with a dry CO_2 atmosphere.

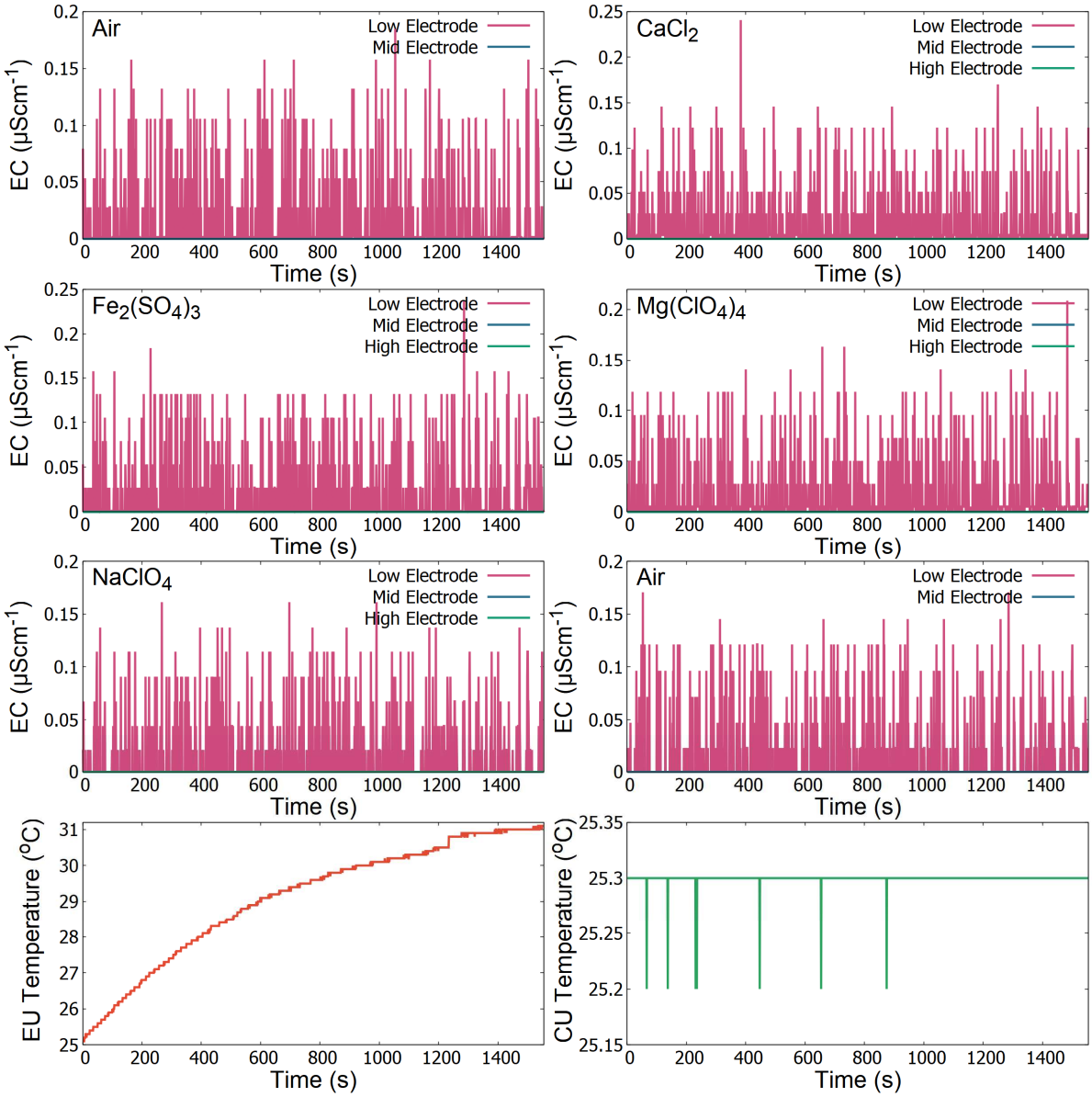

Figure 30: BOTTLE measurement of 1) electric conductivity of the empty containers with Earth ambient air, and the containers with salts and Earth ambient air. These data were measured on 2019/12/06 in the clean-room of TAS-F, during integration on the Surface Platform.

Just before launch, the sealing lid will be replaced with the BOTTLE lid with the HEPA filter that will allow the atmospheric moisture to interact with the salts. We will continue to monitor the EC values during the three health check campaigns that are foreseen to take place during the cruise phase, where this value is expected to drop to the minimum level as the containers

will be exposed to vacuum. The environmental conditions during the cruise will have no implications on the operation of HABIT on Mars. In the uneventful situation (most of the terrestrial water will be lost during the depressurization at launch) that SAP still holds frozen water, the water will be released once that the mission lands on Mars, because HABIT will be reset, i.e., the heaters will be switched on until the minimum value of conductivity is reached. Future work in the Mars simulation chamber will include a proper characterization of the changes of the martian air EC with varying RH% under martian CO_2 atmospheric conditions and with martian surface pressures.

7. BOTTLE products

All the products were purchased from Sigma Aldrich and are summarized in Table 5. The four deliquescent salts that are contained in the cells of BOTTLE in the HABIT FM have been found on Mars, and their phase diagrams allow to hold liquid conditions under the expected temperature range of Oxia Planum. Additionally, these salts have been chosen because their response to the Earth environment is such that it allows for long storage under clean room conditions without initiating deliquescence into liquid. For each salt, the lower temperature which can hold liquid state is indicated in Table 6. The salts are mixed in a 2:1 ratio with a Super Absorbent Polymer (SAP) hydrogel. SAP is made of cross-linked networks of hydrophilic polymer, which on Earth are capable of absorbing from liquid water, 400 times approximately or more of its weight. The SAP used in HABIT is the Poly (Acrylamide-co-Acrylic Acid) with a grain size ranging from 200-1000 μm. The containers are separated from the at-

mosphere through a HEPA filter, to comply with Planetary Protection requirements. The HEPA filter allows the free flow of molecules of the air while impeding the possible flow of micro-organisms and particulate of size greater than 0.3 μm. This is commonly used in clean room facilities and is also implemented in the REMS pressure sensor chimney, as a filter for the air towards the inner part of the rover. Figure 31 shows the HEPA filter assembly of the Flight Model HABIT- BOTTLE experiment.

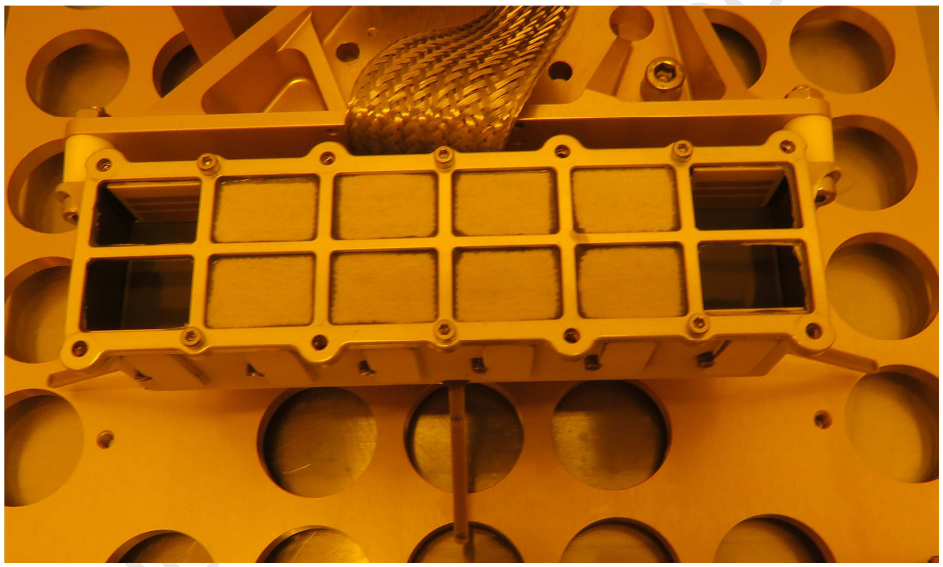

Figure 31: HEPA Filter Assembly of HABIT glued and screwed to the BOTTLE structure using six M2 bolts.

The SAP when mixed with a salt sample, as shown in Figure 32, supports the normal deliquescence of the salt and induces the formation a viscous jelly state, as observed in Figure 33, which inhibits the capillarity of the salts along the walls of the container**.** Additionally, the mixture with SAP allows to measure the electrical conductivity and the repeated absorption and release of water vapour with the atmosphere as in a porous regolith or soil matrix, mimicking the behaviour of the martian regolith. A set of tests (not shown) have been applied to

these mixtures to demonstrate that they retain their water absorption properties, after application of the Planetary Protection Protocols of Dry Heat Microbial-bioburden Reduction (DHMR) and the depressurization caused during the launch and cruise phase (Mathanlal et. al, 2020). Additionally, the swelling ratio of sterilized and depressurized SAP was compared and demonstrated to be equal to the unperturbed commercial SAP (not shown). This demonstrates the capability of SAP to be used for water storage in space applications, in particular at martian pressure conditions and exposed to diurnal and seasonal thermal changes (Mathanlal et. al, 2020).

Table 5: BOTTLE products

Cell #	Product formula	Product name	Total dry weight (g)
1	Empty air/dust	Air at martian pressures and collected mineral dust	-
2	$CaCl_2$: $C_6H_8KNO_3$	Calcium chloride + SAP	2.25
3	$Fe_2(SO_4)_3$: $C_6H_8KNO_3$	Ferric Sulphate +SAP	2.25
4	$Mg(ClO_4)_2$: $C_6H_8KNO_3$	Magnesium Perchlorate + SAP	2.25
5	$NaClO_4$:	Sodium Perchlorate + SAP	2.25

	$C_6H_8KNO_3$		
6	Empty air/dust	Air at martian pressures and collected mineral dust	-

Table 6: Eutectic temperatures and relative humidity's of the chosen salts.

Salt	**Te (K)**	**RH (%)**	**Reference**
$NaClO_4$	236	53	Hennings et al. (2013a,b).
$CaCl_2$	226	60	Toner et. al., 2014
$Mg(ClO_4)_2$	206	52	Stillman and Grimm (2011)
$Fe_2(SO_4)_3$	246.35	40	Hennings et al., 2013a

Figure 32: Illustration of the state of the products after DHMR and depressurization, as they are put on the BOTTLE containers. From left to right, mixtures of SAP with Calcium Chloride (container 2), Ferric Sulphate (container 5), Magnesium Perchlorate (container 3) and

Sodium Perchlorate (container 4). These containers were left outdoors exposed to the ambient temperature and humidity conditions to determine their water absorption capability.

Figure 33: After three days of Earth outdoor exposure, the products have absorbed water from atmosphere and are in a jelly state. For this specific day, the environmental conditions were such that supported deliquescence of Calcium Chloride and this, mixed with SAP, formed a hydrogel. The other salts appear in hydrated state.

In order to avoid deliquescence of the BOTTLE products during its storage on Earth, and to allow for all the stages of assembly, including the upside-down configuration, a solid aluminium lid with a specially designed gasket made of HT870 silicone has been used in HABIT for all the phases of storage, integration, testing and transportation. The solid lid fixture designed will be replaced with the actual roof of HABIT before flight. Figure 34 (left) shows the solid aluminium lid with the specially designed gasket and the Figure 34 (right) shows the actual roof of HABIT which is the flight ready configuration.

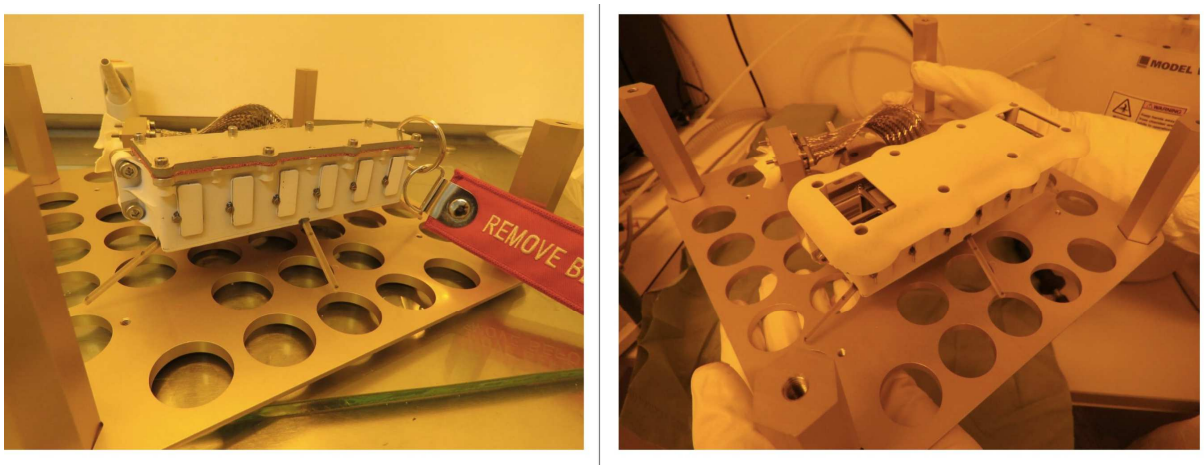

Figure 34: (left) HABIT BOTTLE fitted with the solid aluminium lid and HT870 gasket during the storage phase and (right) HABIT BOTTLE fitted with the roof, which is the flight ready configuration of the HABIT BOTTLE.

Planetary Protection Tests

The ExoMars 2022 mission, landing at Oxia Planum, is designated under Category IVb, following the indications of the European Space Agency (ESA) Planetary Protection Office (PPO), as per the Committee on Space Research (COSPAR) regulation. Category IVb. defines missions with lander systems designed to investigate the extant of martian life without contacting a martian special region. The protocol demands a stringent surface bioburden level of $\leq$ 30 spores. Though the BOTTLE contents are isolated from the exterior environment through the HEPA filter, which prohibits any flow of micro-organism, and any potential biological contamination would be thus considered as encapsulated bioburden, we have applied bioburden reduction procedures to the products of BOTTLE. All the four salt+SAP mixtures have been subjected to Dry Heat Microbial Reduction (DHMR) at 125 °C for 10 hours, to reduce the magnitude of any potential bioburden by 4 to 6 orders magnitude, according to the ECSS-Q-ST-70-57C protocol. To verify the clean level, the salt+SAP mixtures have then been subjected to the standard swab assay procedure as per the ECSS-Q-ST-70-55C protocol.

Figure 35 shows an overview of the swab assay procedure of the Ferric sulphate salt+SAP mixture for determining the microbial colony count after subjecting the salt+SAP mixture to 10 hours of DHMR at 125 °C. The procedure has been performed in a custom made double walled cleanroom tent with a HEPA filtration system (Mathanlal et. al, 2020). Controls were also taken into account during the process to determine the cleanliness of the procedure. As a main certification process, a set of swabs were sent to the Department of Aerospace Medicine, Deutsches Zentrum für Luft- und Raumfahrt (DLR), Germany to assay and determine the colony counts. The products of the swabs were then incubated at 32 °C for three days and the colony count was analysed at 24-hour, 48-hour and 72-hour mark. The test results from DLR further confirmed the cleanliness of the salts with zero colony counts. Additionally, the HABIT hardware was also sterilized and tested, with probes showing also with compliance with the PP requirements.

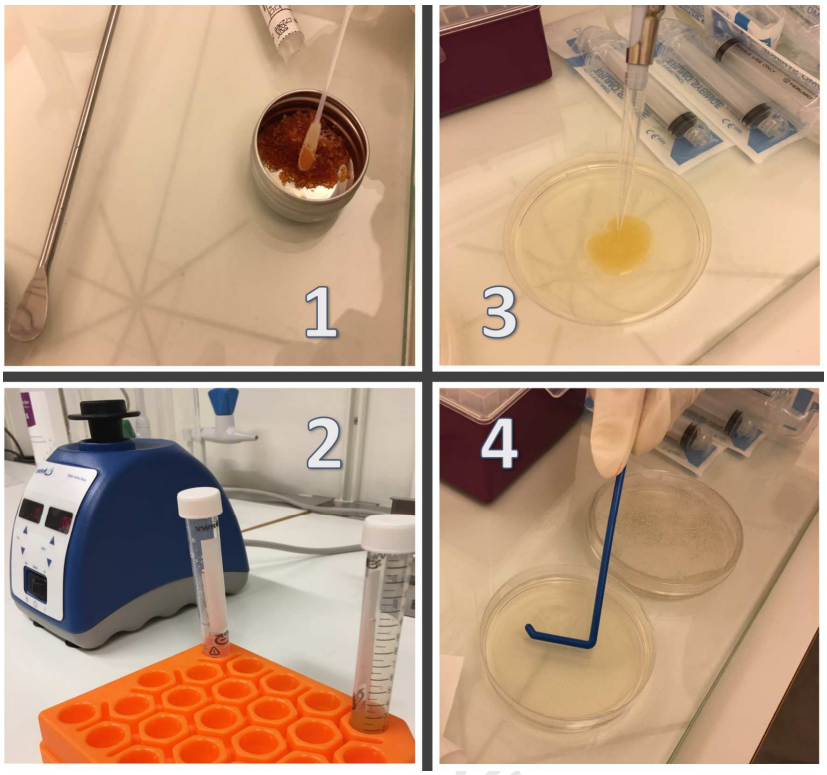

Figure 35: 1). Swabbing the surface of the Ferric Sulphate salt+SAP mixture with nylon tipped FLOQSwab 2). The swabs are then suspended in 2.5ml of sterile Phosphate Buffer Saline (PBS) 3). After the vortex and thermal shock procedure, 0.5ml of the sample pipetted on to R2A petri dish. 4). Spreading the sample with sterile spreader prior to incubation.

Since the products in BOTTLE will probably form brines at relatively mild temperatures, the planetary protection measurements are especially important here. In parallel, as double blind assay, for the products of BOTTLE we performed studies with an equivalent set of swabs and incubated them after spreading them over R2A petri dishes. It could be found that there was no colony observed in the salt+SAP mixture after 72 hours. The BOTTLE contents have thus met the Category IVb. planetary protection requirements and the organics (SAP) are contained in a HEPA-encapsulated environment.

8. HABIT operations and data archiving

8.1 HABIT operation modes

HABIT has two sampling modes: i) the nominal mode, that measures every second within the first 5 minutes of each hour; ii) the extended mode, during which the instrument will measure data for every second during a maximum time-lapse of 3 hours. After that, it will switch to the nominal mode again.

HABIT expects to receive a command every day from the Surface Platform BIP (acronym for the Onboard Information and Memory unit, in Russian) with an updated schedule, specifying for instance when the extended acquisition starts or if the heaters of the CU should be switched on, for how long and with how much intensity. If no command is sent, it will apply by default the last schedule. Additionally, during the cruise phase to Mars, HABIT will be turned on at least twice for autonomous functional tests. The duration of these tests can be limited to a few minutes without the need to go on regular or extended mode (just three packets are needed for health-check tests: the initial data packet, a self-check packet and a sensor data packet, which can be received within one minute). When HABIT is powered up, it initializes its own time by receiving it from the surface platform's (SP) interface and memory unit (BIP), which transmits to HABIT the schedule for operations for the next sol or sols. HABIT has a safety procedure to identify when the received command contains an error, for instance if a parameter is set out of range it is set by default to its maximum allowed value. The transmitted data files include self-check flags (binary variables that point for instance to out of range values). Self-check routines of the brines and temperature electronics take place at the beginning of every session using its own resistors. The current of each cell is also verified with self-check resistor to detect if the calibration is drifting or if some electronic function is not working properly.

8.2 HABIT scientific data outputs and units, for every second of acquisition

HABIT will provide the following measurement: air temperature 1 (K), air temperature 2 (K), air temperature 3 (K), wind 1 (m/s), wind 2 (m/s), wind 3 (m/s), ground temperature (K), UVA (W/m^2), UVB (W/m^2), UVC (W/m^2), UVD (W/m^2), UVE (W/m^2), UVABC (W/m^2), Electrical Conductivity (S/m) level 1 and 2 of air-cells 1 and 6, Electrical Conductivity (S/m) level 1, 2 and 3 of cells 2 to 5 (deliquescent salts, absorbing atmospheric water).

8.3 HABIT data budget

HABIT stores all data packets (science data, engineering and scheduled operations) within its non-volatile (NAND) 512MB flash memory. The expected amount of data acquired per sol (assuming an extended acquisition of 3 hours) is 764 packets, each packet is 2032 bytes size resulting in a total of 1.5 MB/sol. The data are saved in HABIT even when the power is turned off. BIP, once per sol, will request all stored data (science and engineering data) to HABIT and send it to the Surface Platform's onboard computer in binary format, from here the data are sent to Earth through the satellite relay. Upon successful transmission to the surface platform's BIP, HABIT's memory pointer will go to the next register, keeping the transmitted data in the previous one. This register is easily accessible again in case it is needed to send the data yet to BIP. HABIT will only delete data from its memory once it is full, starting from the oldest to the most recent one. HABIT will be able to store up to 330 sols in its internal memory; hence, in case there is any miscommunication between BIP and HABIT, it will be able to work autonomously for many sols.

8.3 HABIT power budget

The power consumption of HABIT can be calculated with the following equation, the first term is the power required for the operation of the EU, 2.1 W, the second term is the power used when the heater of the CU is activated. The resistance of the CU heater is $R_{CUheater}$ = 131 Ohm. The CU heater operates with pulse width modulation (PWM) and its amplitude can be modulated by modifying the intensity with the duty cycle (D) factor, that can be commanded and varies between 0, when no heating is activated on the CU, and 1, when a dedicated dehydration cycle is programmed for the BOTTLE containers. The last term is the power required to heat the EU when the temperature drops below -33°C. The EU heater can be switched on by the autonomous start-up logic or by the EU logic. The EU logic will enable the EU heater when the EU temperature is below -33℃ ± 1℃ and disable if the temperature rises above -30℃ ± 1℃.

$$P_{Avg} = P_{EU} + \frac{(U_{in} * D)^2}{R_{CUHeater}} + \frac{{U_{in}}^2}{R_{EUHeater}}$$

where D = 0 to 1.00

$R_{CUheater}$ *= 131 Ohm*

$R_{EUheater}$ *= 249 Ohm*

U_{in} *= 28 V*

P_{EU} *= 2.1W*

Thus, the power consumption of HABIT is 2.1 W, but when the heaters are activated to their maximal power it can reach 13.1 W.

8.4 HABIT data structure

The data obtained with HABIT will be archived at the IKI/Roscosmos Archive and will be mirrored at the Planetary Science Archive (PSA) (https://www.cosmos.esa.int/web/psa/psa-

introduction) of the European Space Agency (ESA) using the Planetary Data System (PDS) version 4 (PDS4) format standard created by NASA. This archiving protocol is used in all current NASA and ESA space missions along with other international agencies that are members of the International Planetary Data Alliance (IPDA) (https://planetarydata.org/). HABIT produces four levels of data:

- Raw: Received directly from IKI/Roscosmos in binary format, there is no telemetry on them, just the surface platform timestamp and HABIT data. The size of this file is approximately 350 KB.
- Partially processed: During operations, right after receiving the raw data, HABIT binary data is converted into a column-based comma-separated ASCII data file without any calibration. The size of this file is approximately 10 MB containing 39 columns.
- Calibrated: Using the partially processed data and applying the instrument sensors calibration functions, we create the calibrated version of the data. The size of this file is approximately 20 MB containing 50 columns.
- Derived: To create the final scientific version of the data we must combine ancillary data that HABIT does not measure by itself and the calibrated data that we calculated previously. This level needs external information which is stored in the ancillary file, such as solar zenith angle (SZA), or ambient pressure (P). The size of this file is 24 MB containing 65 columns. The HABIT processed data that will be stored at PSA will also include quality flags check for UV dust, UV shadow, UV angle blindness, noise for electronic conductivity and ATS errors.

The downlinked data will be processed daily by the Ground Software HABIT Team, using the calibration functions of the sensors and electronics of HABIT. This transformation shall be

implemented on a daily basis, during operations. Then following the ExoMars data policy, the files shall be delivered as a bundle, including the XML product labels, to be archived at the PSA. Every HABIT bundle will include all the data, ancillary information and other files related to the instrument. In Figure 36 we show an example of a bundle made with the PDS4 standard.

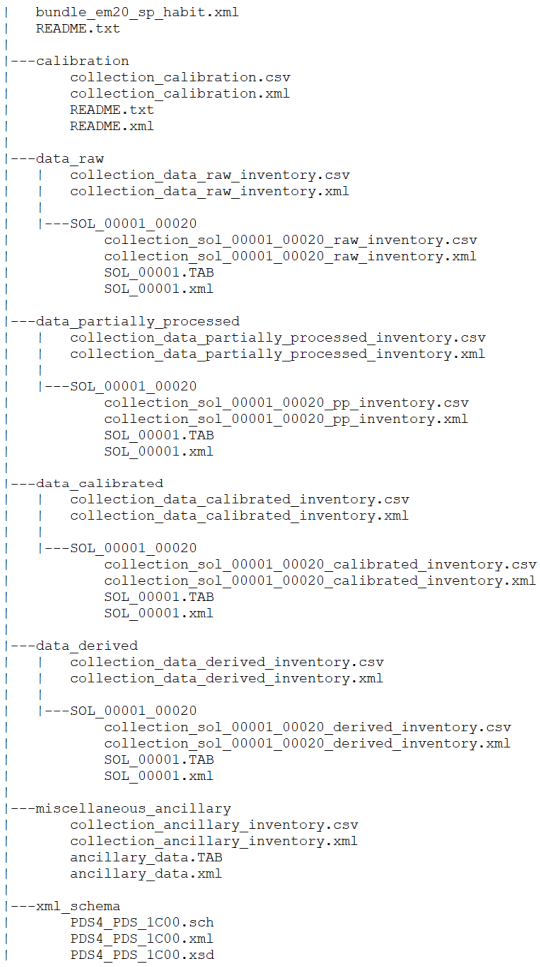

Figure 36: Example of HABIT PDS4 Bundle

9. Operation on Mars, simulations on a Mars environmental chamber

To validate HABIT operations on Mars we have developed the SpaceQ chamber, see Figure 37 (Vakkada-Ramachandran et al., 2019). This chamber is designed to operate instrumentation in representative space conditions (vacuum, Mars atmosphere, Earth stratosphere, lunar environment, etc.) and to validate their performance by acquiring real-time data in a simulated environment. It is also designed to test and qualify the behaviour of certain components when exposed to thermal vacuum, outgassing, baking, low temperatures and dry heat microbial reduction procedures.

One of the main functionalities of the SpaceQ chamber is to recreate locally certain conditions of the Mars surface for research purposes, in this case to operate HABIT as on Mars. The chamber can mimic the diurnal variation of temperature and the water cycle within a thin atmosphere of CO_2 as on Mars. A unique feature of this chamber is that it includes connectors for USB and DB25 to read the data from the instrumentation while being tested inside.

The SpaceQ chamber is a versatile facility which can operate with a wide range of temperatures from 193 K to 423 K and pressure from ambient to $< 10^{-5}$mbar. It is a cubical chamber made of stainless steel with internal volume of 27 l having multiple viewports, feedthroughs and flanges. In order to get the chamber down to vacuum we use rotary pump which pumps down the air to 10^{-3}mbar, if we need to achieve higher orders of vacuum, we then use a turbo molecular pump to reach 10^{-5}mbar. The pressure inside is monitored by a cold cathode/pirani combination gauge which is connected to the display unit and records the values in real time.

There are two gas inlets one used to inject CO_2 gas and other to inject water using a stainless-steel syringe connected via a ball valve to the Swagelok on the chamber. The instrument placed inside the chamber can be communicated in real time with the USB and DB 25 pins fitted on the chamber ports. The temperature of the chamber is maintained in two ways i) cooling: the working table is fitted with a feedthrough to circulate liquid nitrogen in order cool it down to 193 K ii) heating: the chamber wall from outside is fitted with the heating jackets which raise the temperatures up to 423 K. A Vaisala HMT 334 probe which is used for vacuum applications to monitor RH/T of the air inside the chamber. The chamber also has a provision to do visible/near infra-red VNIR spectroscopy as the chamber walls are fitted with the feedthrough to connect the probes of the spectrometer and obtain the spectra of the samples inside. The SpaceQ chamber has been used to simulate the launch phase, cruise phase, and operation of HABIT on the surface of Mars and will be further used to investigate the different responses of the BOTTLE unit of HABIT depending on the angle of inclination, thermal cycles, etc.

Table 7: Specifications of the SpaceQ chamber

Parameter	Characteristics
Internal volume	27 litres
Operating temperature	-80°C to + 150 °C
Operating pressure	ambient to < 10^{-5} mbar
UV lamp	115-400 nm
Data output connectors	USB and DB 25
Vaisala RH/T sensor	0-100% and -70°C to +180°C
Gas/fluid inlet	CO_2 and water

Spectrometers	VNIR 200-1100 nm and 1000 nm-2500 nm

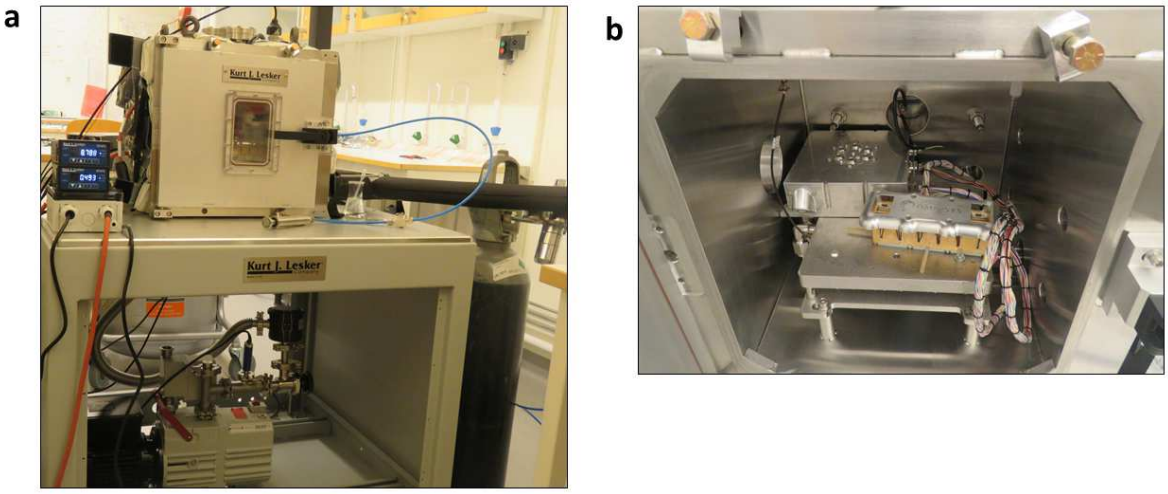

Figure 37: SpaceQ chamber facility: (a) SpaceQ chamber with the rotary pump, syringe used to inject water, CO_2 cylinder and the pressure display (b) HABIT EM placed on the working table and integrated with the DB 25 pin for operation. This table is refrigerated with liquid N_2.

9.1 Mars Sol simulation

We simulated a plausible martian day-night cycle with the HABIT Engineering Model (EM) inside the SpaceQ chamber while controlling the temperature, relative humidity and carbon-dioxide atmosphere identical to the ExoMars 2022 landing site, Oxia Planum. We evacuated out the ambient air from the chamber using a rotary vacuum pump to attain about pressures in orders of 10^{-3} mbar followed by a gentle increase in pressure with carbon-dioxide atmosphere

and maintained it between 6 mbar. We then injected water using a vacuum grade syringe in increments of 0.5 ml at a time, to increase the air relative humidity gradually over 80%. It required up to 20 water injection cycles to achieve the desired initial air relative humidity of 86 %. The working table where HABIT was accommodated was then cooled by injecting LN_2 until BOTTLE temperature (denoted as TCU in Figure 38) reached 243 K (203 K in working table). As the working table cools down, frost starts to form on the table and the relative humidity of the air is reduced. Based on REMS observations on board the Curiosity rover, this is just what is expected to happen on Mars, where the ground will generally be much cooler than the surface platform and the air above. The cooling was then cut off for the chamber to warm up again to ambient temperature of about 293 K. As the table temperature increases water is released to the air, which produces an increase in the RH%. Once the table temperature reaches ambient temperature the experiment is stopped. The progression of the martian simulated environmental conditions during the experiment is shown in Figure 38. We also calculated the relative humidity for water with respect to ice (RH_{CU}^{i}) and liquid (RH_{CU}^{l}) phases for the temperatures of the container unit to estimate the relative humidity to which the salts are exposed.

The BOTTLE EM was initially filled with salt-SAP mixtures in the same configuration and same amounts as in the flight model, with the only modification of using a salt also in Cell-6 instead of leaving it empty. In the process as the table temperature crosses the triple point of water the frost turns into liquid droplets which then evaporate, and the relative humidity of the air starts to raise. The increment in EC of the salt containers indicated that some salts were absorbing water through hydration or deliquescence.

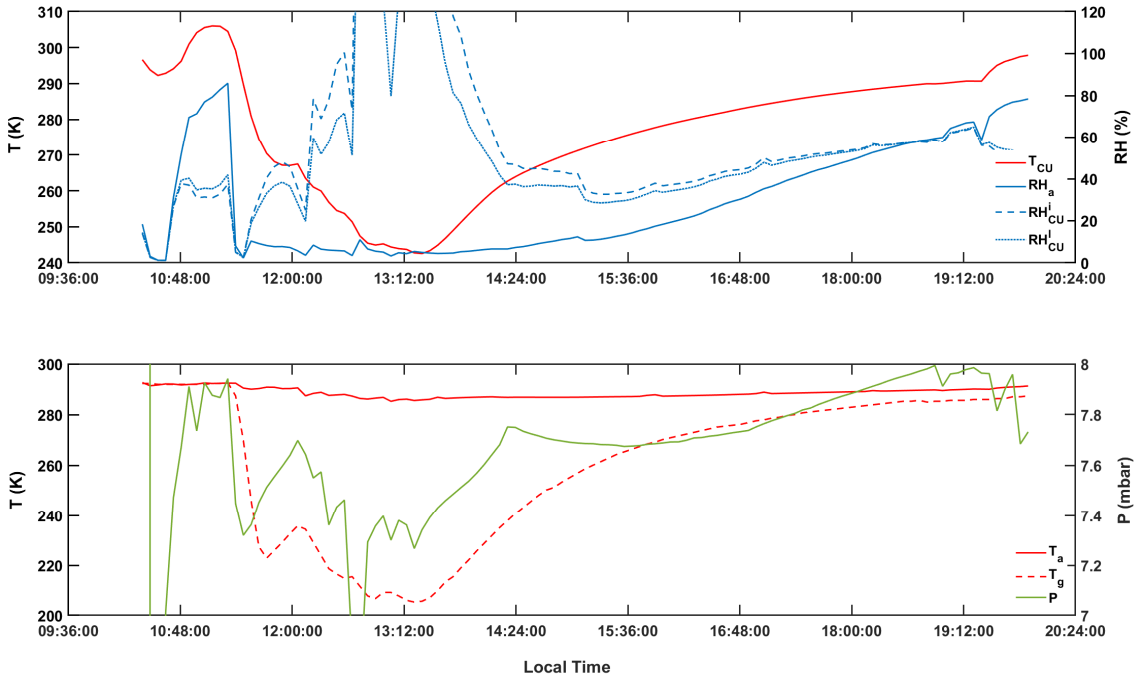

Figure 38: Simulated environment inside the SpaceQ chamber. Different variables recorded such as temperature of both air (T_a) and BOTTLE temperature (T_{CU}), pressure (P), relative humidity of air (RHa) and relative humidity at which BOTTLE salts are exposed, calculated with respect to ice (RH_{CU}^{i}) and liquid (RH_{CU}^{l}).

Figure 39 shows the electrical conductivity measurements of the salt-SAP mixtures during the martian day-night simulation. We could observe two distinguishable EC characteristics corresponding to the water capture, one at the beginning and one towards the end of the simulation. When the relative humidity of the air was increased to 86% as the water was injected, we see a spike in the electrical conductivity values. This behaviour lasted for a short time until the moment when the relative humidity reduced due to cooling and the table acted as a sink, where frost was formed. Cell-1 which was empty also showed this behaviour probing that the EC measurements are sensitive to the air relative humidity. As the temperature of the chamber increased, water was released from the cold table, and the air relative humidity increased too. This allowed favourable conditions for the salt-SAP mixtures to capture water which resulted

in a gradual increase in the EC values. Both of these EC increases were complemented with a visible increase in the BOTTLE (CU) temperature –which is not observed in the EU- due to the exothermic nature of the deliquescence process.

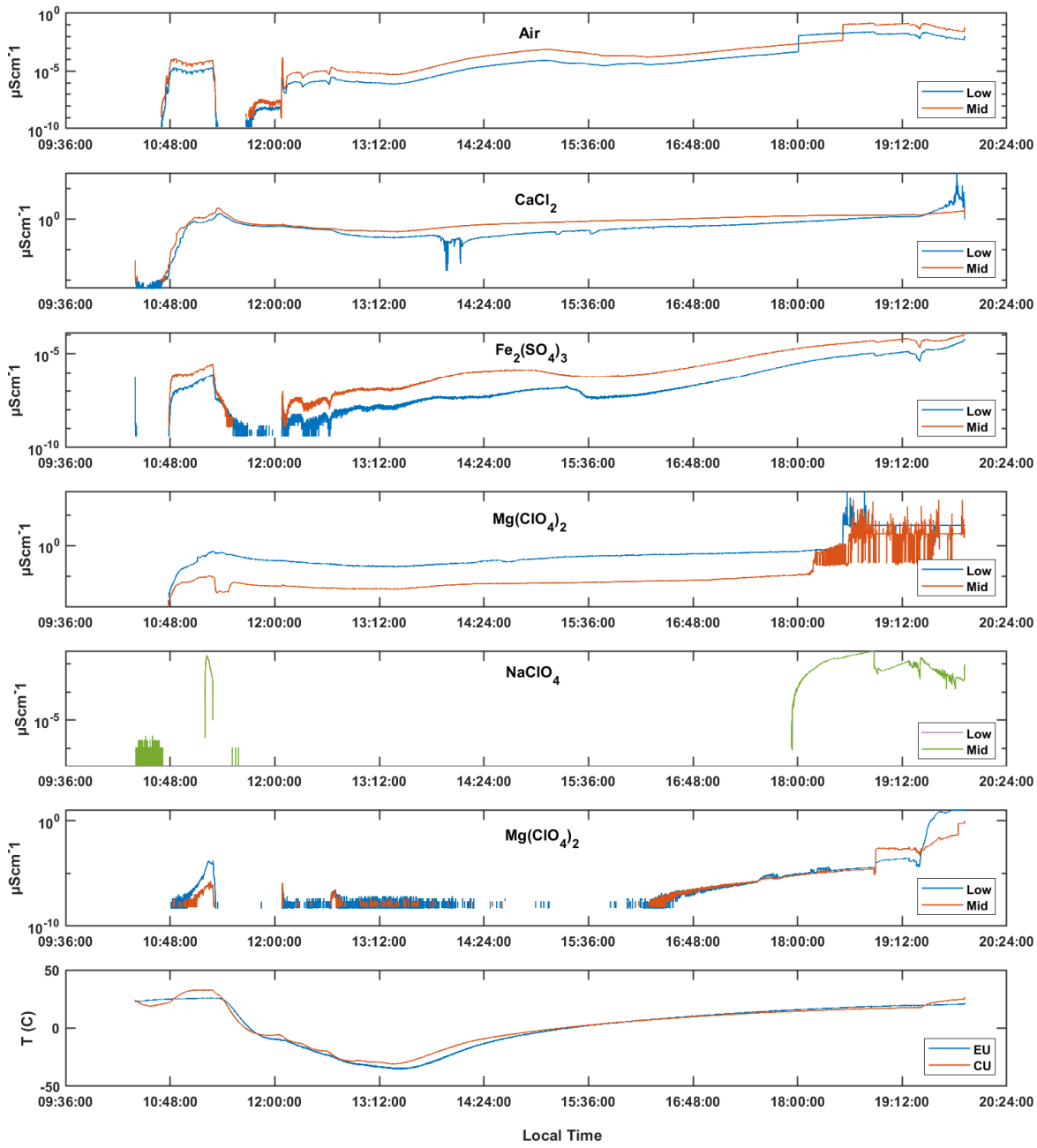

Figure 39: Electrical conductivity measurement (in log scale) of the salts in BOTTLE Engineering Model during the Mars Sol simulation in the SpaceQ chamber. For this experiment the salts were distributed as, Cell-1: Empty, Cell-2: $CaCl_2$, Cell-3: $Fe_2(SO_4)_3$, Cell-4: Mg $(ClO_4)_2$, Cell-5: $NaClO_4$, Cell-6: Mg $(ClO_4)_2$. This experiment simulates HABIT for the study

during its launch and cruise phase with a more representative diurnal variation on Oxia Planum, Mars.

10. Summary

This manuscript describes the instrument HABIT, its operation, and calibration and retrieval procedures that shall be applied to convert the raw data into scientific meaningful variables. HABIT operation has been analysed under laboratory conditions, and dedicated chambers, in order to simulate the different environments where it will be operating. HABIT has been integrated in the ExoMars Surface Platform *Kazachok*, and once in operations on Mars the data will be archived and shared publicly through the Planetary Science Archive (ESA).

HABIT is composed by 2 modules: EnvPack and BOTTLE. The EnvPack module has heritage from previous missions operating on the surface of Mars, and the sensors environmental observations will be directly comparable with those provided by other landed missions on Mars. In HABIT, the implementation of the ATS, GTS and UVS has been adapted to the requirements of the Surface Platform but their observations can be directly compared with those acquired by REMS, on board the Curiosity rover. HABIT can provide information of the local temperature with +/-0.2°C accuracy, local winds with +/- 0.3 m/s, surface brightness temperature with +/- 0.8°C, incident UV irradiance with 10% error of its absolute value in the UVA, UVB, UVC ranges, as well as in the total UVABC range, and two additionally wavebands, dedicated to ozone absorption. The BOTTLE experiment is unique in its kind. The potential transient or permanent existence of brines on Mars, has been controversial and this experiment will provide ground-truth to this hypothesis, by monitoring their response in a controlled environment. Our experiments in a Mars simulation chamber demonstrate that the salts

can absorb water within a few hours of exposure to increased ambient humidity, and that this water can be indirectly monitored by the changes of electric conductivity. Our tests illustrate how BOTTLE can monitor the hydration state of a set of four salts, which have been found on Mars, calcium chloride, ferric sulphate, magnesium perchlorate and sodium perchlorate by measuring their electric conductivity (EC). The EC of the air and the dry salts within the Flight Model under Earth ambient, clean room conditions has been shown to be of the order of 0.1 μScm^{-1} whereas for vacuum conditions it is of the order of 0.00364 μScm^{-1} at ambient temperatures. We have simulated the operation of HABIT, within an environmental chamber, under martian conditions similar to those expected at the ExoMars landing site, in Oxia Planum. For dry CO_2 conditions, at low temperatures, the measured air EC can be as low as 10^{-8} μScm^{-1}, however it increases with RH%. For this specific experiment, after an increase from 0 to 60% RH, within a few hours, the EC of the air increased up to 10^{-1} μScm^{-1}, while magnesium perchlorate hydrated and reached values of 10 $\mu Scm^{-}1$ and calcium chloride deliquesced forming a liquid state with EC of 10^{2} μScm^{-1}. The EC of the other two salts was comparable to the one of the air, indicating that the EC of the air within the voids between salt grains is the dominant component and none, or a negligible amount of hydration has taken place. This comparison between the conductivity of the salts and that of the air, shall always be done on Mars, since all the experiments are exposed to the same temperature and ambient humidity. The products of BOTTLE have been treated with Dry Heat Microbial Reduction sterilization protocols and have passed the ESA planetary protection controls showing no viable cells. Furthermore, our studies demonstrate that the swelling ratio of thermally heated and depressurized SAP was equal to the one of unperturbed commercial SAP suggesting that SAP can be used for water storage in space applications, in particular at martian pressure conditions and exposed to diurnal and seasonal thermal changes (Mathanlal et. al, 2020).

In addition to these tests under laboratory conditions, to demonstrate the operation under non-controlled planetary environments, two engineering prototypes of HABIT have been tested at two international field-campaigns, one in the Himalaya region, a cold and arid environment, (Pandey et al., 2019) and another one in a subsurface environment, with very constant dry conditions (Cockell et al., 2018).

The temperature range of HABIT operation, about -30°C, is coincident with the reported limiting temperatures for cell metabolism and reproduction activity, and thus detecting brine formation at these temperatures will have strong implications for the habitability of present day Mars and also on the future planetary protection considerations that should be applied to sites where brines may be formed.

The observations provided by HABIT may have synergies with other instruments of the rover and SP (http://exploration.esa.int/mars/56933-exomars-2020-surface-platform/). The meteorological station of the SP, METEO-SP, includes Pressure (P) and Relative Humidity (RH) sensors whose measurement shall be complementary to those of HABIT. Additionally, the atmospheric composition observations of FAST-SP, a spectrometer, and MGAP-SP, a GCMS, may be complemented with the UV measurements of HABIT, as on Mars the atmospheric concentration of certain species changes through seasons due to UV-induced photochemistry. Regarding the interaction of the subsurface and near surface with the atmosphere, any seasonal or diurnal variation of the observations of ADRON (which monitors the subsurface water) should be compared with the observations of BOTTLE of the electric conductivity changes of the air and the state of hydrate, frozen brine or liquid brine of the salts in the containers. The near surface winds and temperatures may be compared with the winds of the anemometer and the air temperature of the METEO-SP payload, which is mounted at a higher level on the

mast. The near surface heat-flux depends on the vertical thermal gradients and winds and monitoring this at two points near the surface is critical to provide this information at the boundary layer. The ground temperatures may be compared with the radio thermometer PAT-M for soil temperatures, and the diurnal profile should be used to model the ground thermal inertia which in turn may be correlated with the presence of subsurface ices, that may be potentially detected by ADRON or the radar of WISDOM (in the rover). The atmospheric dust cycle may be observed in the UV by HABIT, and compared with the observations of the PanCam instrument, the camera of the rover, and the studies of dust cycle may be complemented with the observations of the Dust Suite instrument of the platform which determines size, impact and the atmospheric charge. Furthermore, the studies of hydration and surface-atmosphere water interchange may have implications on the hydration state of surface and subsurface minerals. This may be monitored in coordinated campaigns with ISEM and Mi_MASS on the rover, which monitor the IR spectra of minerals. The EC measurements of the air, within the protected environment of the BOTTLE unit, can be compared with those provided by the Dust Suite of the open air on the Surface Platform. The near surface dust observations of MicroMED about the dust cycle and the typical particle size can be compared with the studies of the total column of the atmosphere provided by HABIT combining the measured spectral dependence of the absorbed UV radiation with radiative transfer models. The relative humidity changes observed by the METEO package can be compared with the long-term EC variations of the air. The UV 200-400 nm observations shall be compared with those provided by the 250-400 nm measurements of SIS on the Surface Platform. Additionally, the comparison of HABIT observations with those provided by MEDA on the NASA Perseverance Rover 2020, and REMS on the NASA Curiosity Rover, will provide three simultaneous and similar data sets of environmental observations at different latitudes and longitudes

on Mars that may be used as ground truth validation for orbiter observations and to compare with global and meso-scalar atmospheric modelling and radiative transfer models.

Acknowledgements

HABIT is an instrument of the Luleå University of Technology (LTU), led by J. Martín-Torres (PI) and M-P. Zorzano (co-PI). The international list of Co-Is and collaborators of the science team of HABIT is given in (https://atmospheres.research.ltu.se/habit/pages/team.php). HABIT engineering team: A. Soria-Salinas, M. I. Nazarious, S. Konatham, T. Mathanlal and A. Vakkada Ramachandran. HABIT IT team: J. –A. Ramirez-Luque and R. Mantas-Nakhai. ASS acknowledges the support of the LTU Graduate School of Space. M-P. Z's contribution has been partially supported by the Spanish State Research Agency (AEI) Project No. MDM-2017-0737 Unidad de Excelencia "María de Maeztu" - Centro de Astrobiología (INTA-CSIC). The HABIT FM and EQM were fabricated by Omnisys Instruments AB, based in Gothenburg, Sweden, under advice of LTU as part of the HABIT project development and funded by the Swedish National Space Agency (SNSA). We thank the ExoMars project team, European Space Agency (ESA), Roscosmos, Space Research Institute (IKI) and Omnisys Instruments AB for their hard work on the ExoMars mission. We thank Petra Rettberg and Carina Fink from DLR for their planetary protection analysis of HABIT samples. We acknowledge the Luleå University of Technology, the Wallenberg Foundation and the Kempe Foundation for support of the Mars research activities. We thank the support of the Swedish Institute for Space Physics (IRF) for the TVAC tests. The Oxia Planum environmental conditions research was partially funded by

the European Research Foundation. The SpaceQ chamber has been developed together with Kurt J. Lesker Company and was funded by the Kempe Foundation.

Author Disclosure Statement

No competing financial interests exist.

References

Bhardwaj, A., Sam, L., Martin-Torres, F.J., Zorzano, M.P., 2019, Are slope streaks indicative of global-scale aqueous processes on contemporary Mars?, Reviews of Geophysics, published online, DOI: 10.1029/2018RG000617.

Bhardwaj, A., Lydia Sam, Javier Martin-Torres, Maria-Paz Zorzano, 2019 *Distribution and morphologies of Transverse Aeolian Ridges in ExoMars 2020 Rover landing site,* Remote Sensing in Support of Aeolian Research. DOI: 10.3390/rs11080912

Cockell, C.S., John Holt, Jim Campbell, et. al., 2018, Subsurface scientific exploration of extraterrestrial environments (MINAR 5): analogue science, technology and education in the Boulby Mine, UK, International Journal of Astrobiology, on line, doi: 10.1017/S1473550418000186.

Davis, W. L., I. de Pater, and C. P. McKay, Rain infiltration and crust formation in the extreme arid zone of the Atacama Desert, Chile, Planet. Space Sci., 58(4) (2010) 616–622. https://doi.org/10.1016/j.pss.2009.08.011.

Depiesse, C., Bernd Funke, Maia Garcia-Comas, Jean-Claude Gérard, Marco Giuranna, Francisco Gonzalez-Galindo, Alexey V. Grigoriev, Yuriy S. Ivanov, Jacek Kaminski, Ozgur Karatekin, Franck Lefèvre, Stephen Lewis, Manuel López-Puertas, Arnaud Mahieux, Igor Maslov, Jon Mason, Michael J. Mumma, Lori Neary, eddy Neefs, Andrey Patrakeev, Dmitry Patsaev, Bojan ristic, Séverine robert, Frédéric Schmidt, Alexey Shakun, Nicholas A. teanby, Sébastien Viscardy, Yannick Willame, James Whiteway, Valérie Wilquet, Michael J. Wolff, Giancarlo Bellucci, Manish r. Patel, Jose-Juan López-Moreno, François Forget, Colin F. Wilson, Håkan Svedhem, Jorge L. Vago, Daniel rodionov & NOMAD Science team and ACS Science team, 2019 martian dust storm impact on atmospheric H2O and D/H observed by ExoMars Trace Gas Orbiter, Nature. https://doi.org/10.1038/s41586-019-1097-3

Dundas, C.M., 2020. An aeolian grainflow model for Martian Recurring Slope Lineae, Icarus 343 (2020), 113681, https://doi.org/10.1016/j.icarus.2020.113681

Fand, R. M., Keswani, K. K., 1972. A continuous correlation equation for heat transfer from cylinders to air in crossflow for Reynolds numbers from 10^{-2} to $2x10^{5}$. Int. J. Heat Mass Transf. 15 (3), 559–572.

Fonseca, F., M.-P. Zorzano, J. Martín-Torres. MarsWRF Prediction of Entry Descent Landing Profiles: Applications to Mars Exploration. (2019), Earth and Space Science vol. 5, issue 8, pages 1440-1459, https://doi.org/10.1029/2019EA000575

1686 Gómez-Elvira, J., Armiens, C., Castañer, L., Domínguez, M., Genzer, M., Gómez, F., Haberle,
1687 R., Harri, A.-M., Jiménez, V., Kahanpää, H., Kowalski, L., Lepinette, A., Martín, J., Martínez-
1688 Frías, J., McEwan, I., Mora, L., Moreno, J., Navarro, S., de Pablo, M.A., Peinado, V., Peña,
1689 A., Polkko, J., Ramos, M., Rennó, N. O., Ricart, J., Richardson, M., Rodríguez-Manfredi, J.,
1690 Romeral, J., Sebastián, E., Serrano, J., de la Torre Juárez, M., Torres, J., Torrero, F., Urquí, R.,
1691 Vázquez, L., Velasco, T., Verdasca, J., Zorzano, M.-P., and Martín-Torres, J. (2012) REMS:
1692 The Environmental Sensor Suite for the Mars Science Laboratory Rover. *Space Sci Rev*
1693 170:583-640.
1694
1695 Gómez-Elvira, J., 2013a. Mars Science Laboratory Rover Environmental Monitoring Station
1696 RDR, NASA Planetary Data System Data V1.0, MSL–M–REMS–6–ADR–V1.0.
1697 Gómez-Elvira, J., 2013b. Mars Science Laboratory Rover Environmental Monitoring Station
1698 RDR, NASA Planetary Data System Data V1.0, MSL–M–REMS–4–ENVEDR–V1.0.
1699 Gómez-Elvira, J., 2013c. Mars Science Laboratory Rover Environmental Monitoring Station
1700 RDR, NASA Planetary Data System Data V1.0, MSL–M–REMS–5–MODRDR–V1.0.
1701 Gómez-Elvira, J., Armiens, C., Carrasco, I., Genzer, M., Gómez, F., Haberle, R., Hamilton, V.
1702 E., Harri, A.-M., Kahanpää, H., Kemppinen, O., Lepinette, A., Soler, J. M., Martín-Torres, J.,
1703 Martínez-Frías, J., Mischna, M., Mora, L., Navarro, S., Newman, C., de Pablo, M.A.,
1704 Peinado, V., Polkko, J., Rafkin, S.C.R., Ramos, M., Rennó, N.O., Richardson, M., Rodríguez-
1705 Manfredi, J. A., Romeral Planelló, J. J., Sebastián, E., de la Torre Juárez, M., Torres, J., Urquí,
1706 R., Vasavada, A.R., Verdasca, J., and Zorzano, M.-P. (2014) Curiosity's rover environmental
1707 monitoring station: Overview of the first 100 sols. *J Geophys Res Planets* 119:1680-1688.
1708

1709 Heinz, J., D. Schulze-Makuch, and S. P. Kounaves, Deliquescence induced wetting and RSL-
1710 like darkening of a Mars analogue soil containing various perchlorate and chloride salts, Ge-
1711 ophys. Res. Lett. 43 (2016) 4880–4884. https://doi.org/10.1002/2016GL068919.
1712
1713 Hardgrove, C., Rennó, N.O., Chevrier, V.F., Mischna, M., Navarro-González, R., Martínez-
1714 Frías, J., Conrad, P., McConnochie, T., Cockell, C., Berger, G., Vasavada, A.R., Summer, D.,
1715 and Vaniman, D. (2015) Transient liquid water and water activity at Gale crater on Mars. *Nat*
1716 *Geosci* **8**:357-361.
1717
1718 Holstein-Rathlou, C., Gunnlaugsson, H. P., Merrison, J. P., Bean, K. M., Cantor, B. A., Da-
1719 vis, J. A., Davy, R. et al. (2010), 'Winds at the Phoenix landing site', J. Geophys. Res.
1720 115(E00E18).

1721 Korablev, O., Ann Carine Vandaele, Franck Montmessin, Anna A. Fedorova , Alexander
1722 Trokhimovskiy, François Forget, Franck Lefèvre, Frank Daerden, Ian R. Thomas, Loïc
1723 Trompet, Justin T. Erwin, Shohei Aoki , Séverine Robert , Lori Neary, Sébastien Viscardy,
1724 Alexey V. Grigoriev, Nikolay I. Ignatiev, Alexey Shakun, Andrey Patrakeev, Denis A.
1725 Belyaev, Jean-Loup Bertaux, Kevin S. Olsen, Lucio Baggio, Juan Alday, Yuriy S. Ivanov,
1726 Bojan Ristic, Jon Mason, Yannick Willame, Cédric Depiesse, Laszlo Hetey, Sophie
1727 Berkenbosch, Roland Clairquin, Claudio Queirolo, Bram Beeckman, Eddy Neefs, Manish R.
1728 Patel , Giancarlo Bellucci, Jose-Juan López-Moreno, Colin F. Wilson, Giuseppe Etiope, Lev
1729 Zelenyi , Håkan Svedhem, Jorge L. Vago & The ACS & NOMAD Team, 2019, No detection
1730 of methane on Mars from early ExoMars Trace Gas Orbiter observations, Nature. DOI:
1731 10.1038/s41586-019-1096-4
1732
1733 Mathanlal, T., Nazarious, N.I. Ramachandran, A. V., Zorzano, M.-P., Martin-Torres, J., 2020

Implementing Bioburden reduction and control on the Deliquesecent hydrogel of the HABIT/ExoMars 2022 Instrument, Acta Astronautica, https://doi.org/10.1016/j.actaastro.2020.04.030

McAdams, W. H., 1954. Heat transmission, 3rd Edition. New York : McGraw-Hill

McAdams, W. H., 1954. Heat transmission, 3rd Edition. New York : McGraw-Hill

McKay, C. P., E. I. Friedmann, B. Gómez-Silva, L. Cáceres-Villanueva, D. T. Andersen, and R. Landheim, Temperature and moisture conditions for life in the extreme arid region of the Atacama desert: Four years of observations including the El Niño of 1997–1998, Astrobiology, 3(2) (2003) 393–406. https://doi.org/10.1089/153110703769016460.

Merrison, J., BechtoldH, H., Gunnlaugsson, H., Jesen, A., Kinch, K., Nornberg, P. and Rasmussen, K. (2008), `An environmental simulation wind tunnel for studying Aeolian transport on mars', Space Sci. Rev. 56(3-4), 426-437.

Martín-Torres, J., Zorzano, M.-P., Valentín-Serrano, P., Harri, A.-M., Genzer, M., Kemppinen, O., Rivera-Valentin, E.G., Jun, I., Wray, J., Bo Madsen, M., Goetz, W., McEwen, A.S.,

Mueller, D. and Abu-Mulaweh, H. (2006), Prediction of the temperature in a fin cooled by natural convection and radiation, Appl. Therm. Eng. 26, 1662-1668

Nazarious et al., Calibration and preliminary tests of the Brine Observation Transition To Liquid Experiment on HABIT/ExoMars 2020 for demonstration of liquid water stability on Mars. Acta Astronautica, 162 (2019) 497-510. https://doi.org/10.1016/j.actaastro.2019.06.026

1758 Okajima, A. (1990), 'Numerical Simulation of the Flow Around Rectangular Cylinders', J.
1759 Wind Eng. Ind. Aerod. 33(1-2), 171-180.

1760 Pandey, S., Jonathan Clarke, Preeti Nema, Rosalba BonaccorsiSanjoy Som, Mukund Sharma,
1761 Binita Phartiyal, Sudha Rajamani, Rakesh Mogul, Javier Martin-Torres,
1762 Parag Vaishampayan, Jennifer Blank, Luke Steller, Anushree Srivastava1, Randheer Singh,
1763 Savannah McGuirk, María-Paz Zorzano, Johannes Milan Güttler, Teresa Mendaza, Alvaro
1764 Soria-Salinas, Shamim Ahmed, Arif Ansari, Veeru Kant Singh, Chaitanya Mungi, Niraja
1765 Bapat, Ladakh: Diverse, High-Altitude Extreme Environments for Off- Earth Analogue and
1766 Astrobiology Research. International Journal of Astrobiology. In print 2019.
1767

1768 Perkins, H. C., Leppert, J. G., 1964. Local heat-transfer coefficients on a uniformly heated
1769 cylinder. Int. J. Heat Mass Transf. 7 (2), 143–158.

1770 Rummel, J.D., Beaty, D.W., Jones, M.A., Bakermans, C., Barlow, N.G., Boston, P.J.,
1771 Chevrier, V.F., Clark, B.C., de Vera, J.P., Gough, R.V., Hallsworth, J.E., Head, J.W., Hipkin,
1772 V.J., Kieft, T.L., McEwen, A.S., Mellon, M.T., Mikucki, J.A., Nicholson, W.L., Omelon,
1773 C.R., Peterson, R., Roden, E.E., Sherwood Lollar, B., Tanaka, K.L., Viola, D. and Wray J.J.
1774 (2014) A new analysis of Mars "Special Regions": findings of the second MEPAG Special
1775 Regions Science Analysis Group SR-SAG2). Astrobiology 14:887-968.
1776

1777 Sebastián, E., Armiens, C., Gómez-Elvira, J., Zorzano, M.P., Martinez-Frias, J., Esteban, B.,
1778 and M., Ramos, The Rover Environmental Monitoring Station Ground Temperature Sensor:
1779 A Pyrometer for Measuring Ground Temperature on Mars. (2010) Sensors, 10, 9211-9231.
1780 doi:10.3390/s101009211
1781

1782 Soria-Salinas, A., Zorzano, M.-P., Mantas-Nakhai, R., Martín-Torres, J., 'Wind retrieval from
1783 temperature measurements from the Rover Environmental Monitoring Station/Mars Science
1784 Laboratory', Icarus (under review).

1785 Soria-Salinas, A., Zorzano, M.-P-, Martín-Torres, J., 'The wind sensor of the HABIT instru-
1786 ment for Mars', Exp. Therm. Fluid Sci. (under review).

1787 Vago, J.L., Westall, F., Pasteur Instrument Teams, Landing Site Selection Working Group,
1788 and Other Contributors. (2017). Habitability on early Mars and the search for biosignatures
1789 with the ExoMars Rover. Astrobiology 17:471–510.
1790
1791 Vandaele et al., 2019 ***Martian dust storm impact on atmospheric H2O and D/H observed by***
1792 ***ExoMars Trace Gas Orbiter,*** Nature. DOI: 10.1038/s41586-019-1097-3
1793
1794 Vakkada Ramachandran, A., Miracle Israel Nazarious, Thasshwin Mathanlal, María-Paz Zor-
1795 zano, Javier Martín-Torres. SpaceQ chamber: the environment simulator for planetary explo-
1796 ration instrumentation and research, EPSC Abstracts Vol. 13, EPSC-DPS2019-PREVIEW,
1797 2019 EPSC-DPS Joint Meeting 15-20 September 2019, Geneva, Switzerland
1798
1799 Vakkada Ramachandran, A. M.-P. Zorzano, J. Martín-Torres, The stability of Martian dew
1800 and brines under non-equilibrium conditions, Scientific reports (under review)
1801
1802 Van Der Hegge Zijnen, B. G., 1956. Modified correlation formulae for the heat transfers by
1803 natural and by forced convection from horizontal cylinders. Appl. Sci. Res. 6 (2-3), 129–140.

Yang, L., Pabalan, R. T., Juckett, M. R. Deliquescence Relative Humidity Measurements Using an Electrical Conductivity Method, Journal of Solution Chemistry 35(4) (2006) 583-604. https://doi.org/10.1007/s10953-005-9015-8

Zorzano, L. Vázquez, S. Jiménez. (2009). "Retrieval of ultraviolet spectral irradiance from filtered photodiode measurements", Inverse Problems vol. 25, issue 11, pp: 115023-115032

HiGhlights

- The HABIT instrument will characterise the present-day habitability at the ExoMars 2020 landing site
- HABIT will investigate the existence of liquid water on Mars in the form of brines, for how long, and the water-regolith cycle.
- HABIT will investigate the conductivity of atmospheric dust on Mars
- The module BOTTLE will be the first European In-situ Resource Utilization instrument on Mars. It will produce liquid water for future Mars exploration

Declaration of interests

☒ The authors declare that they have no known competing financial interests or personal relationships that could have appeared to influence the work reported in this paper.

☐The authors declare the following financial interests/personal relationships which may be considered as potential competing interests: